

Integration of natural data within a numerical model of ablative subduction: A possible interpretation for the Alpine dynamics of the Austroalpine crust.

Manuel Roda

Università degli Studi di Milano, Dipartimento di Scienze della Terra “A. Desio”, now at Universiteit Utrecht, Faculty of Geosciences, Budapestlaan 4, 3584 CD Utrecht, THE NETHERLANDS

Corresponding author. E-mail: jediroda@gmail.com

Maria Iole Spalla

Università degli Studi di Milano, Dipartimento di Scienze della Terra “A. Desio”, Sezione di Geologia, Via Mangiagalli 34, 20133 Milano - ITALY

IDPA, CNR, Via Mangiagalli, 34, I-20133 Milan, Italy

Anna Maria Marotta

Università degli Studi di Milano, Dipartimento di Scienze della Terra “A. Desio”, Sezione di Geofisica, Via L. Cicognara 7, 20129 Milano - ITALY

IDPA, CNR, Via Mangiagalli, 34, I-20133 Milan, Italy

Short title: Model of ablative subduction in the Alps.

1 **ABSTRACT**

2 A numerical modelling approach is used to validate the physical and geo-
3 logical reliability of the ablative subduction mechanism during Alpine con-
4 vergence in order to interpret the tectonic and metamorphic evolution of an
5 inner portion of the Alpine belt: the Austroalpine Domain. The model pre-
6 dictions and the natural data for the Austroalpine of the Western Alps agree
7 very well in terms of P - T peak conditions, relative chronology of peak and
8 exhumation events, P - T - t paths, thermal gradients and the tectonic evolu-
9 tion of the continental rocks. These findings suggest that a pre-collisional
10 evolution of this domain, with the burial of the continental rocks (induced
11 by ablative subduction of the overriding Adria plate) and their exhumation
12 (driven by an upwelling flow generated in a hydrated mantle wedge) could be
13 a valid mechanism that reproduces the actual tectono-metamorphic config-
14 uration of this part of the Alps. There is less agreement between the model
15 predictions and the natural data for the Austroalpine of the Central-Eastern
16 Alps. Based on the natural data available in the literature, a critical discus-
17 sion of the other proposed mechanisms is presented, and additional geological
18 factors that should be considered within the numerical model are suggested
19 to improve the fitting to the numerical results; these factors include varia-
20 tions in the continental and/or oceanic thickness, variation of the subduction
21 rate and/or slab dip, the initial thermal state of the passive margin, the oc-
22 currence of continental collision and an oblique convergence.

23 **Key words:** ablative subduction; numerical modelling; hydrated mantle
24 wedge; European Alps; Austroalpine Domain.

25 INTRODUCTION

26 The exhumation of *HP-UHP* continental rocks is a topic that has intrigued
27 many geoscientists since the late 1960's. Based on depth-time paths analy-
28 sis and analogue and numerical modelling, pre-collisional and syn- to post-
29 collisional exhumation mechanisms have been proposed (e.g. Duchêne *et al.*,
30 1997). In the first case, exhumation occurs in an accretionary wedge (e.g.
31 Yamato *et al.*, 2007), in regions of corner flow (e.g. Cloos, 1982; Shreve &
32 Cloos, 1986; Cloos & Shreve, 1988) and in the serpentinised mantle chan-
33 nel (wedge) (e.g. Gerya & Stöckhert, 2005; Meda *et al.*, 2010; Roda *et al.*,
34 2010). Crust-mantle delamination (e.g. Chemenda *et al.*, 1995), continent or
35 micro-continent collision (e.g. Gerya *et al.*, 2008; Warren *et al.*, 2008), slab
36 break-off (Ernst *et al.*, 1997), slab retreat (Ring & Layer, 2003), rollback
37 slab (Brun & Faccenna, 2008), intra-continental subduction (e.g. Schuster &
38 Frank, 1999; Thöni, 2006; Janak *et al.*, 2009; Stüwe & Schuster, 2010) and
39 vertical extrusion leaded by rigid mantle indentation (Rolland *et al.*, 2000;
40 Schwartz *et al.*, 2007; Schreiber *et al.*, 2010) are mechanisms that have been
41 proposed to drive syn- to post-collisional exhumation.

42 Natural data and numerical predictions indicate that peculiar thermal
43 and kinematic features characterise the uplift path of continental rocks ex-
44 humed via different mechanisms. Rocks exhumed before the collision show
45 cold prograde and retrograde paths, metamorphic peak imprints that are
46 mainly recorded under *HP* and subordinate *UHP* conditions and contrast-
47 ing metamorphic evolution recorded by adjacent portions of the same struc-
48 tural nappe (Spalla *et al.*, 1996; Gerya & Stöckhert, 2005; Engi *et al.*, 2001;
49 Meda *et al.*, 2010). Furthermore, pre-collisional exhumation occurs within

50 low viscosity and/or low-density complexes, and the exhumation rate ranges
51 from slow to moderate (Roda *et al.*, 2010).

52 Rocks exhumed during or after the onset of collision generally show
53 warmer prograde and exhumation paths in which the retrograde trajectory
54 can be isothermal or characterised by heating during decompression, depend-
55 ing on whether the uplift occurs during early or late in the collision. In these
56 cases amphibolite facies re-equilibration is mainly predicted with the local
57 occurrence of partial melting. The metamorphic peaks record *HP* and *UHP*
58 conditions and the exhumation rates range from medium to high (Ernst &
59 Liou, 2008; Guillot *et al.*, 2009).

60 Although these features have been widely described in *HP-UHP* oro-
61 genic belts, some controversies persist regarding the individuation of the ef-
62 fective exhumation mechanisms of subducted continental rocks. The debate
63 regarding the mechanisms proposed for the exhumation of the Austroalpine
64 continental crust in the European Alps is still open. The Austroalpine Do-
65 main is mainly composed of continental metamorphic, igneous and sedimen-
66 tary rocks derived from the distal part of the African passive continental mar-
67 gin (the Adria plate), involved in the Alpine subduction since the Cretaceous
68 (early Alpine, Spalla *et al.* (2010) and references therein). Although there is a
69 general recognition that these rocks have been involved in Alpine subduction-
70 collision, their contrasting tectono-thermal evolutions and structural setting
71 have generated different interpretations of Alpine geodynamics (e.g. Polino
72 *et al.*, 1990; Spalla *et al.*, 1996; Beltrando *et al.*, 2010), as discussed in the
73 following section. The identification of the exhumation mechanisms affecting
74 the orogenic belts requires the correct evaluation of the actual dimensions

75 of crustal and/or mantle portions that share a similar tectono-metamorphic
76 evolution after their coupling (e.g. Spalla *et al.*, 2010). This topic remains
77 under debate within the Alpine (e.g. Spalla *et al.*, 1996; Schwartz *et al.*,
78 2000; Rosenbaum & Lister, 2005) and extra-Alpine (e.g. Schneider *et al.*,
79 2004; Blanco-Quintero *et al.*, 2011) scientific community.

80 To contribute to this debate, a numerical model of ablative subduction
81 (e.g. Polino *et al.*, 1990; Spalla *et al.*, 1996; Meda *et al.*, 2010; Roda *et al.*,
82 2010, 2011) with hydrated mantle wedge in an ocean-continent system is
83 performed to compare, for the first time, the results with the natural data
84 obtained for the entire Austroalpine Domain in terms of P - T peak estimates,
85 relative peak chronology and exhumation time, P - T - t paths, thermal gra-
86 dients and the geodynamic evolution of the continental rocks. In addition,
87 we infer the volume of those parts that likely share the same tectonic and
88 thermal history from peak to exhumation. Other proposed mechanisms are
89 also discussed, based on the natural data collected and a brief comparison
90 with present-day ocean-continent subduction in North America is proposed.

91 **THE AUSTRALPINE DOMAIN**

92 The uppermost tectonic domain of the Alpine belt is composed of Aus-
93 troalpine continental rocks that tectonically overlie the Penninic Domain
94 (Figs 1 and 2). The latter consists of mixed oceanic and continental slices
95 and containing the remnants of the Tethyan domain. The western termi-
96 nation of the Austroalpine units is located at the northern boundary of the
97 Lanzo Ultramafic Massif and the eastern termination coincides with the east-
98 ern border of the chain (Pannonian Basin). In the western portion of the

99 belt, the Austroalpine rocks also occur in small slivers mingled with conti-
100 nental and oceanic units of the Penninic Domain. In the following sections,
101 the tectono-metamorphic evolution of the Austroalpine Domain will be sum-
102 marised by considering three different parts (Fig. 1): (1) the Austroalpine
103 of the Western Alps outcropping to the west of the Lepontine Dome; (2) the
104 Austroalpine of the Central Alps between the Lepontine Dome to the west
105 and the Tauern Window to the east; (3) the Austroalpine of the Eastern Alps
106 that outcrops to the east of the Tauern Window.

107 The internal structure of the Austroalpine domain (Fig. 2), reveals a
108 heterogeneous lithostratigraphy of the units, characterized by different meta-
109 morphic evolutions, both in Western and Eastern sectors of the chain. The
110 metamorphic evolution of the Austroalpine basement indicates that numer-
111 ous portions, located along the entire length of the chain, have been deeply
112 involved in subduction processes (e.g. Bousquet *et al.*, 2004; Thöni, 2006) be-
113 cause they display an eclogite- to *HP*-amphibolite-facies metamorphism, as
114 well shown in the Map of the Metamorphic Structure of the Alps (Oberhänsli
115 , 2004). The P/T ratios inferred for the eclogitic imprint generally increase
116 from east to west, suggesting that the subduction setting of the Western
117 Austroalpine is generally colder than the Eastern Austroalpine (Fig. 3a).
118 However, highly-contrasting P/T ratios can be observed in the same struc-
119 tural units in the entire Austroalpine Domain (i.e. the Sesia-Lanzo zone
120 (SLZ), Fig. 3a). Metamorphic ages inferred for the eclogitic imprint of the
121 Eastern Austroalpine are older than those obtained for the western part (e.g.
122 Bousquet *et al.*, 2004; Handy & Oberhänsli, 2004), suggesting that the con-
123 tinental crust was involved in subduction in this portion of the Alpine belt

124 earlier than in the Western Alps (Fig. 3b).

125 **The Austroalpine domain of the Western Alps**

126 Alpine evolution in the Austroalpine domain of the Western Alps (AWA) is
127 characterised by polyphase deformation under blueschist- to eclogite-facies
128 conditions followed by retrogression under blueschist- to successive greenschist-
129 facies conditions (e.g. Meda *et al.*, 2010). For the Sesia-Lanzo zone (SLZ),
130 mineral ages ranging between 60 and 80 Ma (Fig. 3 and Table 1) have been
131 related to the Alpine eclogite facies peak (e.g. Lardeaux & Spalla, 1991; Inger
132 *et al.*, 1996; Duchêne *et al.*, 1997; Rubatto, 1998; Rubatto *et al.*, 1999; Rebay
133 & Spalla, 2001; Rubatto *et al.*, 2011). The P -peak values, which are widely
134 dispersed, range between 1.0 and 2.5 GPa, and the maximum estimated value
135 of T is approximately 650–680° (Fig. 4a). For the External Slices (Dal Piaz
136 *et al.*, 2003), lower P -peaks have been estimated with mineral ages ranging
137 from 40 to 50 Ma (Fig. 3 and Table 1).

138 Contrasting P - T and P - T - d - t evolutions have been inferred based on
139 phase equilibria calculations and geothermometry (Castelli *et al.* (2007), and
140 references therein) for different parts of the complex, which experienced a
141 metamorphic imprint from eclogite to greenschists facies (e.g. Andreoli *et al.*,
142 1976; Dal Piaz *et al.*, 1983; Kienast, 1983; Tropper & Essene, 2002; Hellwig,
143 2003; Babist *et al.*, 2006; Rebay & Messiga, 2007; Roda & Zucali, 2008; Gosso
144 *et al.*, 2010), Fig. 4). The P - T - t paths involve high dP/dT conditions and
145 lawsonite can occur in assemblages developed during prograde or retrograde
146 trajectories (Zucali & Spalla (2011), and references therein). The estimated
147 exhumation rates lie in the range 1.4 to 3.5 mm/a (Zucali *et al.*, 2002; Ru-
148 batto *et al.*, 2011). Rubatto *et al.* (2011) suggest that multiple stages of

149 re-equilibration occurred under eclogite facies conditions for the rocks of the
150 Sesia-Lanzo zone, with two subduction-exhumation cycles occurring over 20
151 Ma. Large-scale shear zones developed during the final stages of greenschist
152 facies re-equilibration in central SLZ (Babist *et al.*, 2006) and in the Dent-
153 Blanche klippe (Pennacchioni & Guermani, 1993; Hellwig, 2003; Roda &
154 Zucali, 2008), and a later brittle- ductile faulting postdates the Oligocene
155 andesitic dykes and igneous stocks of the Biella and Traversella emplace-
156 ment in the SLZ (Zanoni *et al.*, 2008, 2010; Zanoni, 2010). Both plutons are
157 emplaced in the innermost part of the SLZ (the Eclogitic Micaschist Com-
158 plex) close to the internal boundary of the Alpine metamorphic units (i.e.,
159 the Periadriatic tectonic line).

160 Natural data related to the metamorphic peak conditions estimated for
161 different portions of the Austroalpine of the Western Alps (reported in Figs
162 1a and 4a and Table 1) indicate the existence of a thermally-depressed en-
163 vironment compatible with active oceanic subduction (the cold subduction
164 of Cloos (1993)), with a low T /depth ratio also maintained during the ex-
165 humation, which is testified by the blueschist re-equilibration following the
166 eclogite facies imprint (e.g. Pognante, 1991). This peculiar metamorphic
167 evolution suggests the interpretation of a burial-exhumation cycle that was
168 accomplished during active oceanic subduction (e.g. Spalla *et al.*, 1996; Zucali
169 *et al.*, 2004; Meda *et al.*, 2010; Roda, 2011).

170 According to other authors, the occurrence of *HP* and *UHP* metamor-
171 phism in the Western Alps can be interpreted as episodic and induced by
172 fast changes from shortening to extension (Rosenbaum & Lister, 2005). In
173 such a tectonic scenario, orogenic processes are governed by the subduction

174 of small ocean basins, slab rollback and the accretion of continental ribbons.
175 In this tectonic configuration, each accretionary event is followed by revival
176 of subduction and slab rollback in an adjacent oceanic basin, which, in turn,
177 would switch the overriding plate into an extensional mode. The latter could
178 then lead to the formation of metamorphic core complexes on the overriding
179 plate and rapid exhumation of *HP* rocks (Rosenbaum & Lister (2005) and
180 references therein).

181 **The Austroalpine domain of the Central Alps**

182 Peak P - T conditions for the eclogite facies event, in the Central Upper Aus-
183 troalpine, have been derived from metabasics and their country rocks at 0.8–
184 1.4 GPa and 500–680°C (Hoinkes *et al.*, 1991; Poli, 1991; Spalla, 1993; Solva
185 *et al.*, 2001; Habler *et al.*, 2006). Zanchetta (2007) suggests the occurrence
186 of *UHP* eclogites (2.6–2.9 GPa and 630–690°C) preserved as boudins within
187 the garnet-amphibolites (Figs 1b and 4b). Recent geochronological data
188 for the age of Cretaceous metamorphism in the Upper Austroalpine nappes
189 range between 76 ± 5 and 85 ± 5 Ma (Solva *et al.*, 2001; Habler *et al.*, 2006;
190 Zanchetta, 2007); an age of 143 ± 2 Ma is inferred by Hoinkes *et al.* (1991)
191 using Rb/Sr ratio on white mica (Fig. 3 and Table 2). A biotite-whole-rock
192 Rb-Sr age of 70–80 Ma indicates that cooling below approximately 300°C
193 occurred during the Upper Cretaceous (Habler *et al.*, 2006).

194 During the Alpine time, a clockwise P - T path is inferred for the Err,
195 Sella and Magna nappes: burial of the continental crust during the Ligure-
196 Piemontese oceanic-crust subduction (between 100 and 80 Ma) and subse-
197 quent multi-stage nappe stacking under high P/T greenschist facies condi-
198 tions are interpreted to have occurred between 80 and 30 Ma (Handy *et al.*,

199 1996). Bachmann *et al.* (2009) indicate an age ranging from 54 to 47 Ma for
200 the cessation of subduction induced by the Middle-Penninic (Brianzonese)
201 collision.

202 With the exception of the Languard-Campo (Gazzola *et al.*, 2000) and
203 Err/Margna nappes (Handy *et al.*, 1996; Konzett & Hoinkes, 1996), the P -
204 T - t paths for this portion record a generally higher thermal state during
205 the early stages of the exhumation with respect to the metamorphic peak
206 (Hoinkes *et al.*, 1991; Habler *et al.*, 2001; Solva *et al.*, 2005; Zanchetta, 2007),
207 reaching amphibolite facies conditions.

208 The structural and metamorphic setting of this portion of the Austroalpine
209 Domain has led to the interpretation of a continuous tectonic erosion of
210 the upper plate in a subduction channel context regarding the Lower Aus-
211 troalpine units (Bachmann *et al.*, 2009). Conversely, for the Upper units, a
212 syn-collisional extruding wedge is proposed by Solva *et al.* (2005).

213 **The Austroalpine domain of the Eastern Alps**

214 The P - T peak estimated for the Eastern Austroalpine exhibits a low P/T
215 ratio, with values of T ranging from 550 to 780°C and P -peak values that
216 vary widely from approximately 1.0 to 2.5 GPa (Figs 1b and 4b). Excluding
217 the Siegraben eclogites and Reckner blueschists unit, there is a marked
218 synchronism of ages for HP metamorphism along the Eastern Austroalpine
219 of 80–90 Ma (Thöni (2006), Fig. 3b and Table 2). The slight difference with
220 respect to the peak-age of the Western Alps led Thöni (2006) to infer that the
221 HP event in the Eastern Alps resulted from a distinct event of continental
222 subduction, probably related to the Meliata-Hallstatt ocean closure (Kurz &
223 Fritz, 2003; Thöni, 2006; Handy *et al.*, 2010). However, Handy *et al.* (2010)

224 note that the Eo-alpine orogenic wedge contains no suture in the classical
225 sense of an ophiolite belt sandwiched between metamorphosed upper and
226 lower-plate units. The only relics of the Meliata-Hallstatt ocean consist of
227 pelagic sediments incorporated in Jurassic-age accretionary wedges (Mandl
228 & Ondrejicka, 1993).

229 The lack of sedimentary material sourced from high-grade metamorphic
230 rocks in the Late Cretaceous (Campanian - Maastrichtian) central Alpine
231 Gosau sediments may indicate a decrease of exhumation rates after approx-
232 imately 85 Ma (Wiesinger *et al.*, 2005; Thöni, 2006) which has been inter-
233 preted as the result of a short-lived (5–7 Ma) high- P event, followed by rapid
234 exhumation (Janak *et al.*, 2009). This view is partly contradicted by that
235 of Tenczer & Stuwe (2003), who show that northern Koralpe and the sur-
236 rounding Austroalpine crystalline basement cooled to below 200°C at 50 Ma
237 (fission track), suggesting a lower exhumation rate than those invoked above.

238 The P – T – t paths for this portion are characterised by a heating during
239 the exhumation or by an isothermal uplift. Alternatively, Gaidies *et al.*
240 (2008a) report an anti-clockwise Alpine P – T path in the Rappold Complex,
241 demonstrating a thermal state during exhumation that was colder than that
242 of the burial event.

243 The exhumation of Eastern Austroalpine units could be related to the
244 occurrence of a back-arc extension during the Ligure-Piemontese subduction
245 successive to the Meliata closure (Kurz & Fritz, 2003) or driven by an ex-
246 truding wedge and erosion during a transpressive regime within an oblique
247 subduction event (Thöni, 2006; Handy *et al.*, 2010).

248 NUMERICAL SIMULATION

249 **Model setup**

250 Submar code (Marotta *et al.*, 2006) is used to simulate the convergence of
251 an ocean-continent system using a grid 1400 km wide by 708 km deep con-
252 taining 6165 nodes and 3010 triangular quadratic elements as described in
253 Roda (2011) and Roda *et al.* (2011). The material properties and rheological
254 laws are summarised in Table 3. Crust and mantle are compositionally dif-
255 ferentiated via the Lagrangian particle technique (Christensen, 1992) with a
256 density of 1 marker (particle) per 0.25 km². To simulate plate convergence,
257 the velocities are fixed at the base of the oceanic crust (a depth of 10 km)
258 with a value of 3 cm/a. To force subduction, we fixed the same velocity at
259 depths up to 100 km at the nodes of the numerical grid distributed along a
260 45° dip plane. We assumed a continental lithosphere thickness of 80 km (with
261 30 km of continental crust) to represent an originally-thinned passive margin
262 that characterised the former margin of Adria (e.g. Dal Piaz, 2001). Using a
263 value of approximately 40 Ma of active spreading for the Ligure-Piemontese
264 ocean (Handy *et al.*, 2010), we assumed 80 km thick oceanic plate following
265 the relation (Turcotte & Schubert, 2002):

$$y = 2.32(kt)^{1/2} \quad (1)$$

266 where y is the thickness of the oceanic lithosphere, k is the thermal dif-
267 fusivity ($10^{-6} \text{ m}^2/\text{s}$) and t is the oceanic plate age.

268 The model runs for 65 Ma of active subduction at time increments of
269 100 ka; the model simulation ends before continental collision. The assumed

270 model constraints cause a strong coupling (i.e. high friction) between the
271 upper and lower plates (see Roda *et al.* (2010) for a discussion of this and
272 additional references); therefore, our models are representative of the sole
273 erosive margin type, which represent, at present, approximately the 60% of
274 the global active margins (Clift & Vannucchi, 2004).

275 **Model results**

276 Figure 5 illustrates the predicted temperature and velocity fields, and the
277 distribution of markers at four time steps. In the early stages of the sub-
278 duction the ablation of the overriding plate by the oceanic plate dominates
279 the subduction dynamics. The high coupling between the two plates inhibits
280 the formation of a large and deep trench, and only a small amount of sed-
281 iment is generated (Fig. 5a). The kinematics are dominated by the burial
282 flow, although some small-scale upwelling flows could develop in the mantle
283 wedge (Fig. 5a, inset). However, the intensity of the upwellings are not able
284 to exhume a large amount of subducted material. With the progression of
285 mantle wedge serpentinitisation (which is due to the continuous subduction
286 and dehydration of the oceanic plate, up to 20 Ma from the beginning of
287 subduction), a more intense upwelling flow develops, especially in the upper
288 part of the mantle wedge (Fig. 5b). Consequently, some crustal and sedi-
289 mentary material is carried up to superficial levels. The sub-horizontal flow
290 generated along the overriding plate maintains the high degree of coupling
291 between the two plates and induces a flexural bending of the continental
292 plate close to the trench with consequent uprising of the lithospheric mantle.
293 The suction generated by the high degree of coupling decreases the slab dip
294 at depths of 200–350 km (Fig. 5b). During the intermediate stages of sub-

295 duction the upwelling flow in the serpentinised mantle wedge becomes the
296 dominant mechanism, the coupling between the two plates decreases and a
297 large trench wedge develops (Fig. 5c). Large amounts of subducted mate-
298 rials are exhumed, and the upper and lower continental slices and sediment
299 particles are involved in the recycling of the mantle wedge. However, only
300 part of the recycled material reaches the surface; the rest remains in the deep
301 portion of the mantle wedge or is more deeply buried (Fig. 5c, light purple,
302 deep purple and yellow markers). Due to the decrease in plate coupling, suc-
303 tion decreases and the slab dip increases in comparison to the previous time
304 increments. The upwelling flow increases the rising of the lithospheric mantle
305 to subsurface levels, and thermal and mechanical erosion of the continental
306 plate occurs.

307 Kinematically, the mantle wedge is characterised by three vortical flows
308 located at depths from 30 to 100 km (Fig. 5c, inset). The late stages are
309 characterised by a stable and highly efficient upwelling flow arising from
310 the widespread serpentinisation of the suprasubductive mantle wedge. The
311 consequence is a large orogenic wedge generated by the accretion of exhumed
312 upper and lower continental crustal slices, recycled trench sediments and
313 particles of upper oceanic crust. Even markers of continental lithospheric
314 mantle are buried and exhumed in the mantle wedge (Fig. 5d, see markers
315 legend). The combined effect of ablation and upwelling flow induces the
316 thermal and mechanical erosion of the overriding plate along a zone extending
317 from 100 to approximately 150 km from the trench, with the consequent
318 denudation of the lower crust (Fig. 5d). The streamline pattern shows a
319 single and intense vortical flow located in the mantle wedge from a depth of

320 30 to approximately 100 km (Fig. 5d, inset).

321 The P - T - t paths followed by the upper and lower continental markers
322 indicate burial of the material during the early stages of subduction and sub-
323 sequent exhumation to subsurface levels and the upper part of the mantle
324 wedge (Fig. 6). The mechanism of burial depends on subduction age; the
325 T/P ratio decreases during the intermediate stages depending on the cooling
326 generated by the progressive subduction of the oceanic plate. Furthermore,
327 because the trajectory of every marker could be characterised by more than
328 one burial-exhumation loop as suggested by the P - T - t paths (Fig. 6), the
329 markers could record different values of P_{Tmax} and T_{max} during their evolu-
330 tion within the mantle wedge and different exhumation rates.

331 Several analyses can be performed taking the exhumed markers into ac-
332 count; in this model, all particles that reach a minimum burial depth of 80 km
333 and are subsequently exhumed to a depth of at least 30 km are considered as
334 exhumed markers. Analysis of the thermo-barometric conditions recorded by
335 the exhumed markers confirms the high variability of the thermo-barometric
336 conditions at maximum pressure ($P_{max}T$), with P_{max} values from 1.2 GPa to
337 up to 3.7 GPa, and of T , ranging from 250 to 600°C (Fig. 7a). The distri-
338 bution of the predicted thermo-barometric conditions recorded at maximum
339 temperature by the markers (PT_{max} , Fig. 7b) also demonstrates high vari-
340 ability of the pressure associated with T_{max} (from 1.0 to 3.5 GPa), but less
341 variation in temperature, which is limited to the range 450–650°C. At the
342 end of the simulation, the upper 50 km of the accretion wedge is composed
343 of 56% mantle and hydrated mantle, 43.5% continental material and 0.5%
344 oceanic material. Markers belonging to the lower continental crust are about

345 17.5% of the total amount of the exhumed material whilst 10% represents
346 the amount of upper continental crust.

347 The thermal-gradients characterising the subduction zone, which are pre-
348 dicted at various reference depths from the minimum values of the depressed
349 geotherms, (Fig. 7c), exhibit the strongest decrease during the early stages of
350 their evolution, followed by a modest decrease during the intermediate stages
351 until a constant value is reached during the late stages. If we consider the
352 sole mantle wedge area (up to 300 km depth), the thermal gradients during
353 the late stages of subduction range from 2 to 4 °C/km. Thermometric deter-
354 mination of *UHP* orogenic peridotites (Ernst & Liou, 2008) corroborate such
355 predicted cold thermal regimes. Furthermore, the mean thermal gradients
356 obtained from the burial path of the markers in the numerical simulation
357 overestimate those extracted from the isotherms, at least during the first 40
358 Ma of subduction (Fig. 7c). Analysis of the P/T ratio, which is obtained
359 from the mean $P_{max}T$ conditions recorded by the exhumed markers at five
360 different time steps (Figs 7d and e), confirms the progressive cooling of the
361 mantle wedge over time during ongoing subduction; the P/T values, which
362 range from approximately 2.5 to 3.6–3.7 (10^{-3} GPa/°C), are equivalent to
363 T/depth values ranging from 13 to 9 °C/km. It is important to emphasise
364 that these P/T ratios do not coincide with the thermal gradients, which
365 are exclusively represented by the configuration of the geotherms at different
366 time steps (Fig. 7c).

367 We calculated the dimensions of the crustal markers groups that experi-
368 enced common $P-T-t$ histories, from the peak to the exhumation (60 Ma
369 from the beginning of the subduction), disregarding their origin (upper or

370 lower crust). Taking into account that each marker represents a homoge-
371 neous area of 0.25 km^2 , we found a maximum group dimension of 53 km^2
372 with a mean value of 11 km^2 . These estimates represent the dimensions of a
373 single metamorphic unit that means a portion of crustal and/or mantle ma-
374 terial that shared a common tectono-thermal history within the exhumation
375 process.

376 **COMPARISON WITH NATURAL DATA**

377 In this section a comparison between model predictions and natural data from
378 the Austroalpine continental crust is presented and the results are critically
379 discussed. Natural data are grouped according to the locality and tectonic
380 units, P - T estimates and peak ages (Figs 1 and 4, Tables 1 and 2). We
381 consider all the particles that have been buried below and recycled above
382 a depth of 30 km (1.0 GPa), which is the starting crustal thickness, to be
383 exhumed continental crust. For this reason, no statistical data are presented
384 below a pressure of 1.0 GPa.

385 **The Austroalpine of the Western Alps**

386 In Fig. 8, the thermo-barometric peak conditions of the natural data for the
387 Austroalpine of the Western Alps are plotted against the numerical results
388 in terms of of Pressure- (Fig. 8a, b) and Temperature- (Fig. 8c, d) peak
389 conditions. Although there is in general good agreement between the P -peak
390 recorded by the rocks and that of the model, the better agreement in terms
391 of temperature is obtained by comparison with the numerical P - T peak
392 conditions referred to the maximum temperature (PT_{max}). The predicted
393 values of T at P_{max} are generally lower than those derived from the natural

394 assemblages, particularly for T -values related to higher maximum pressures
395 (from 1.5 to 2.5 GPa), whereas the T -values estimated for lower maximum
396 pressures (≤ 1.5 GPa) fit well. The comparison of natural data with model
397 results in regard to the PT_{max} are instead ever in very good agreement.
398 This agreement could indicate that the P -peak recorded by the Austroalpine
399 rocks does not correspond to the maximum pressure reached during the rock
400 burial, but could instead be related to the pressure conditions recorded at
401 the maximum temperature, where the kinetics of the metamorphic reactions
402 increase and the phase changes can be more pervasive. Conversely, this could
403 also be due to the lack of sufficiently refined petrological methods able to
404 identify actual pressures instead of minimal pressure conditions and reduce
405 the uncertainty in estimates of T (Fig. 4).

406 If the subduction simulation has a duration that is equivalent to a time-
407 span of 65 Ma, i.e., starting at 95 Ma and ending at 30 Ma, it is possible
408 to compare the simulation results with the timing of P - T peak indicated in
409 the literature. These ages range from 80 to 60 Ma for the SLZ and from
410 50 to 40 Ma for the External Slices (see Table 1 and Figs 2, 8e and f).
411 Although older peak ages were proposed in the literature, the improvement
412 of the dating techniques and the problem related to the excess and/or loss
413 of Argon in the Alpine belt (e.g. Ruffet *et al.*, 1995) suggest that the more
414 recent estimates available and not related to Ar methods are more reliable
415 (see Table 1). Based on geological evidence, part of the subducted material
416 was already exhumed to shallow crustal levels by 30 Ma, and this result is
417 compatible with the development of greenschist facies assemblages at the
418 expense of eclogite facies ones when the subduction ceased at the beginning

419 of continental collision (e.g. Platt, 1986; Polino *et al.*, 1990; Zanoni *et al.*,
420 2010). Following these natural constraints, the end of the model simulation
421 (after 65 Ma, i.e., 30 Ma) is considered to broadly coincide with the age
422 at which exhumation occurs. Based on these assumptions, there is very
423 good agreement temporally between the simulated P - T conditions and the
424 record of the peak conditions in the natural rocks for both the SLZ and
425 External Slices (Figs 8e and f). At the end of the simulation, i.e., at 30 Ma,
426 a large number of the same continental ablated and buried markers have been
427 exhumed to subsurface levels (Figs 8e and f, yellow markers). Some of the
428 markers, however, reside at significant depth at the end of the simulation, and
429 could potentially remain at depth unless exhumed by a subsequent orogenic
430 event.

431 In Fig. 9, a comparison between selected natural and simulated P - T - t
432 paths is proposed that also takes pre-Alpine P - T paths into account, where
433 available in the literature. This is useful for constraining the extraction of
434 the marker trajectories with respect to their starting structural level, at the
435 beginning of the subduction and in the upper or lower crust, based on the
436 results suggested by the pre-Alpine P - T - t natural evolution. Furthermore,
437 we extract the simulated P - T - t paths by considering the time interval cor-
438 responding to the specific Alpine peak age proposed in the literature or, in
439 the absence of radiometric data regarding natural peak assemblages, the P -
440 T - t path recorded during a 80 to 60 Ma time span. Although many P - T - t
441 paths are reported in the literature, we compared the numerical results with
442 P - T - t paths produced since 2000 for which modern and accurate structural
443 and petrological analyses were available. In Fig. 9 the grey area represents

444 the area comprising all the numerical P - T - t trajectories, and the purple and
445 blue lines represent some examples of various paths. Orange and cyan boxes
446 and black arrows refer to the natural P - T conditions (pre-Alpine and Alpine)
447 and natural P - T - t paths, respectively, as given in the literature and noted in
448 the figure legend. Natural and simulated P - T - t paths are generally in good
449 agreement in terms of both prograde and retrograde trajectories with the ex-
450 ception of the External Slice paths Arolla and Mt. Morion (Fig. 9). In these
451 cases, as discussed in the literature, peak conditions are attained close to
452 the onset of continental collision at approximately 30 Ma, (e.g. Zanoni *et al.*,
453 2010; Handy *et al.*, 2010) and consequently the thermal regime, character-
454 ising the exhumation of these rocks, can increase due to high shear heating
455 and strong radioactive decay (e.g. Gerya *et al.*, 2008; Warren *et al.*, 2008).
456 It must also be emphasized that our numerical simulation is stopped before
457 the collision event, and therefore, exhumation is only partially accomplished
458 under a sensible low-temperature regime.

459 **The Austroalpine of the Central Alps**

460 The comparison between the natural and the simulated thermo-barometric
461 conditions of the Central Alps shows no agreement with regard to $P_{max}T$
462 (Figs 10a and b) values because of the higher temperatures retrieved from
463 the natural data. However, the natural data are consistent with the higher
464 simulated T_{max} values in the PT_{max} diagram (Figs 10c and d). The samples
465 that record lower peak-pressure (lower than 1.0 GPa) are not compared to
466 the simulations.

467 For the comparison between the natural age data and the timing of the P -
468 T peak from the model, we extract the simulated P - T values for the first 20

469 Ma of subduction (i.e., from 100 to 80 Ma, as suggested in the literature, Fig.
470 3b and Table 2), and the exhumation age corresponds to 50 to 35 Ma (Handy
471 *et al.*, 1996; Bachmann *et al.*, 2009). Fig. 10e allows a qualitative estimate of
472 fitting percentage between simulated P - T peak values (red dots) and natural
473 estimates (shaded area) of at least 50%. Furthermore, the predicted P - T
474 conditions at the end of simulation (orange dots) are coherent with natural
475 P - T data set and associate age.

476 Only one natural P - T - t path agrees well with the predictions of the
477 model (Fig. 9: “Mortirolo” (ref. 1 Central Alps, Fig. 1b)). Other P -
478 T paths from the literature display a warmer thermal state for both the
479 peak and exhumation conditions and are therefore not consistent with the
480 simulated P - T - t paths.

481 **The Austroalpine of the Eastern Alps**

482 A comparison of the natural and the simulated thermo-barometric conditions
483 of the Eastern Alps shows no agreement with regard to the $P_{max}T$ values
484 and a poor agreement with PT_{max} values due to the higher thermal state
485 suggested by the natural data (Fig. 11). For the Eastern Alps, we considered
486 130 Ma to be the age at which subduction began, based on the peak age of
487 Siegraben (Table 2). In this region, in contrast to the the Western Alps,
488 the P -peak ages lie in the range from 100 Ma to 90 Ma, and two exhumation
489 stages are considered: 80 Ma (Thöni *et al.*, 2008) and 50 Ma (Tenczer &
490 Stuwe, 2003).

491 A low correspondence is obtained between the timing of the P -peak for
492 the Eastern Austroalpine (90–100 Ma) and the model predictions (Fig. 11e).
493 Regarding the peak age interval, good agreement is obtained only for lowest

494 P values. For the higher pressures, a colder thermal state is predicted by
495 the simulation (Fig. 11e). A significant better agreement is found if the
496 subduction beginning is assumed at 100 Ma (excluding Siegraben), and the
497 predicted P - T conditions refer to the early stages of subduction (1–10 Ma
498 = 100–90 Ma, Fig. 11f). Indeed, for this time span, a higher thermal state
499 is predicted than for the intermediate stages of the subduction. In any case,
500 a considerable amount of buried material has already been exhumed at both
501 exhumation time-steps considered, although a large part sinks to greater
502 depths and probably will remain buried.

503 As with the Central Austroalpine, only one natural P - T - t path agrees
504 well with the predictions of the model (Fig. 9: “Sopron” (ref. 19.2 Eastern
505 Alps, Fig. 1c)). In this case, only the peak-pressure is well reproduced,
506 whereas the thermal state of the exhumation path is underestimated by the
507 simulated paths. Other natural P - T paths display a warmer thermal state
508 for both the peak and exhumation conditions and are not reproduced by the
509 simulations.

510 DISCUSSION

511 The model predictions agree well with the natural P - T estimates and the
512 P - T - t paths derived from for the Austroalpine crust of the Western Alps.
513 All natural P - T data are reproduced by the numerical P - T predictions, es-
514 pecially the P - T peak conditions obtained by PT_{max} analysis. Even the time
515 interval between the peak and exhumation conditions are closely consistent
516 with the ages inferred from the rocks, with different P -peak ages, for the SLZ
517 and the External Slices. In this context, the exhumation rate suggested by

518 the numerical model ranges from 0.1 to 1 cm/a, with mean values of 0.3–0.4
519 cm/a. These exhumation rates agree with those predicted by Roda *et al.*
520 (2010) and suggested by Zucali *et al.* (2002) and Rubatto *et al.* (2011) for a
521 part of the SLZ. Good agreement is found between the natural and simulated
522 P – T – t paths, both with and without consideration of their pre-Alpine evolu-
523 tion, with few exceptions. These cases are characterised by a peak-age very
524 close to the collisional event, and their retrograde paths could be affected by
525 the increase of temperature induced by the continental collision.

526 The same heterogeneity that characterises both the natural and predicted
527 P – T peak conditions and the P – T – t evolutions in the same structural domain
528 suggests the juxtaposition of rocks with different metamorphic evolutions.
529 The rocks have been coupled and decoupled at different stages during their
530 trajectories in the mantle wedge (e.g. Spalla *et al.*, 1996; Gerya & Stöckhert,
531 2005; Bousquet, 2008; Roda *et al.*, 2010; Spalla *et al.*, 2010). In this context it
532 is evident that the tectono-metamorphic unit definition requires an evaluation
533 of the actual size of crust and mantle-derived slices that coherently shared,
534 after amalgamation, the same tectonic and thermal history. In light of this,
535 the structural and metamorphic evolutions of basement rocks trace their
536 transit throughout different levels of the lithosphere and sub-lithospheric
537 mantle (e.g. Schwartz *et al.*, 2000, 2007; Spalla *et al.*, 2010; Blanco-Quintero
538 *et al.*, 2011), rather than the purely lithologic associations or the common
539 dominant metamorphic imprint. The tectono-metamorphic unit dimensions
540 obtained in this work are at least one order of magnitude lower than those
541 proposed for the Alps (e.g. Oberhänsli, 2004): this means that the refinement
542 of a method for the identification of contours of thermally-characterized and

543 structurally-distinct units became crucial (Spalla *et al.*, 2005, 2010) to obtain
544 a good definition of the Alpine tectono-metamorphic units. In the case of the
545 Western Austroalpine, the model results and their fitting with the natural
546 data indicate that a nappe (Sesia-Lanzo Zone) can result from the accretion
547 of different tectonic units.

548 The thermal gradient of the simulated subduction zone lies in a range
549 from 2 to 4 °C/km (Fig. 7c). Groppo *et al.* (2009), based on the P - T as-
550 semblages obtained for some samples belonging to the “Lago di Cignana”
551 unit, suggest a gradual decrease in the thermal gradient (from 9–10 to 5–6
552 °C/km) over time. This variation, which is simply related to the time, has
553 been interpreted by these authors as evidence for an increase in the subduc-
554 tion rate of the Ligure-Piemontese oceanic slab during the Eocene. However,
555 a deeper analysis of P - T - t paths reveals that the attribution of thermal gra-
556 dient significance to a single and transient P - T estimate cannot be directly
557 related to the variation of the geotherms. The inference of variation in ther-
558 mal gradients requires a minimum of two P - T estimates and the knowledge
559 of the configuration of isotherms in an evolving dynamic system such as an
560 active subduction zone. Thus, the prograde path inferred by Groppo *et al.*
561 (2009) suggests a thermal gradient of approximately 3 °C/km, which agrees
562 well with that predicted by the numerical model, rather than the transition
563 between two different thermal gradients proposed by the authors. Further-
564 more, the numerical model suggests that the thermal gradients inferred by
565 the burial path of the markers are quite different than those extracted from
566 the isotherms (Fig. 7c). This finding indicates that the determination of
567 thermal gradients that are derived directly from the P - T path could be af-

568 fected by uncertainties arising from the nonlinear trajectories of the markers
569 in the mantle wedge and to variability in the thermal regime.

570 The model results suggest the occurrence of a very dynamic mantle wedge
571 that produces two or three subduction-exhumation loops recorded by the
572 markers within 65 Ma of active subduction (Fig. 6). This aspect of the mod-
573 elling is consistent with the recent discovery of two subduction-exhumation
574 cycles recorded in the same rocks in the Western Austroalpine of the Alps (the
575 Sesia-Lanzo Zone (Rubatto *et al.*, 2011). Similar subduction-exhumation cy-
576 cles have been invoked to justify the complex P - T trajectory inferred for the
577 rocks of the Caribbean subduction channel (Blanco-Quintero *et al.*, 2011)
578 and the Franciscan complexes (Wakabayashi & Dumitru, 2007; Wakabayashi,
579 2011).

580 All of the previous points suggest a pre-collisional evolution of the Aus-
581 troalpine of the Western Alps, involving the burial of slices ablated by the
582 margin of the overriding continental plate (the Adria plate) during subduc-
583 tion and their successive exhumation (driven by the upwelling flow generated
584 in a hydrated mantle wedge).

585 A much more modest agreement between the natural data and model
586 predictions occurs for the evolution of Austroalpine rocks from the Central
587 and Eastern Alps. In these regions, the simulated thermal state is generally
588 underestimated with respect to that derived from P - T estimates of the rocks.
589 Although the timing of simulated P - T peak and exhumation are comparable
590 with those suggested in the literature, only a small part of the predicted P - T
591 conditions is consistent with the natural conditions.

592 These results suggest that entirely pre-collisional ablative mechanisms are

593 unable to explain the high temperature recorded by the rocks belonging to
594 the Austroalpine of the Eastern Alps. A model that includes continental col-
595 lision could better explain the high thermal state reached by the rocks before
596 and during exhumation (Faccenda *et al.*, 2008; Gerya *et al.*, 2008; Warren
597 *et al.*, 2008), although the high levels of mixing of units predicted by the cited
598 models do not appear to reproduce the low level of heterogeneity observed in
599 the Eastern Alps, according to Janak *et al.* (2009). An intra-continental sub-
600 duction zone is the suggested alternative interpretation (Janak *et al.*, 2009).
601 However, a mechanism able to engage an intra-continental subduction is dif-
602 ficult to identify. The thickening of the continental crust of the upper plate
603 is probably a more common mechanism (which is effective during active sub-
604 duction) that could be invoked to explain higher values of T_{max} . Indeed, the
605 influence of a thick upper plate on the thermal state of the wedge has been
606 described in the case of low slab dip and strong plate coupling, where a higher
607 thermal regime characterises the mantle wedge during active subduction be-
608 fore continental collision (Roda *et al.*, 2011). This finding suggests that the
609 higher T values recorded in the Eastern Austroalpine could be related to lat-
610 eral variations of upper plate thickness along the Alpine convergent margin.
611 As noted previously, the thermal state depends on the subduction age (early
612 vs. intermediate subduction, Figs 7d and 11).

613 The poor lithologic heterogeneity assessed in the Eastern Alps is weak-
614 ened by the heterogeneities in the P - T peak conditions and P - T - t evolutions
615 of natural rocks both within single and between different units (Fig. 1 and
616 Table 2). The lithostratigraphic homogeneity that characterises the East-
617 ern Austroalpine with respect to the melange-like assemblage of the Western

618 Austroalpine does not necessarily imply homogeneous and coherent P - T - t -
619 d paths. The lithostratigraphy of the Western Austroalpine is comparable
620 to that described in the Central-Eastern Austroalpine, but a high level of
621 heterogeneity is predicted by the different P - T - t - d evolution recorded by
622 the slices constituting the same structural domain (or “Alpine nappe”) (e.g.
623 Schwartz *et al.*, 2000; Bousquet, 2008; Spalla *et al.*, 2010). In this con-
624 text, better-refined prograde P - T - t paths and, in general, a wide spread
625 in derived P - T - t or P - T - t - d paths are needed for the Austroalpine of the
626 Central-Eastern Alps to allow the existence of possible tectono-metamorphic
627 homogeneities to be discerned.

628 Roda *et al.* (2010, 2011) suggest that a thinned oceanic plate (less than
629 80 km, as reasonable for a young ocean) and/or a variation of the subduction
630 rate and/or the slab dip could affected the thermal state of the mantle wedge.
631 Taking into account an oblique Alpine subduction and the possible V-shape of
632 the Ligure-Piemontese ocean (e.g. Schmid *et al.*, 2004), it should be possible
633 to obtain a decrease of the thermal state of the subduction zone from east
634 to west that is related to an increase in the oceanic plate thickness.

635 However, some natural P - T conditions reflect a very high thermal state,
636 partially consistent with the numerical predictions obtained for the early
637 stages of the subduction. This observation suggests that the initial LP
638 thermal state of the rocks could influence the thermal evolution of buried-
639 exhumed rocks during the subduction. Marotta *et al.* (2009) (and references
640 therein) indicate that the Austroalpine domain is widely affected by HT - LP
641 Permian-Triassic metamorphism, which developed during the early stages
642 of the Tethyan rifting. The subduction of the Eastern Austroalpine crust

643 earlier than that of the Western Austroalpine crust could imply a thermally
644 perturbed continental margin, a younger (and therefore hotter) oceanic plate
645 and a higher T/P ratio in the early stages of the subduction.

646 Moreover, horizontal movement linked to transpressive subduction could
647 affect the $P-T$ conditions recorded during the exhumation paths, as noted
648 by Thompson *et al.* (1997a,b). In this case, the exhumation is characterized
649 by a transition from blueschist to granulite facies conditions consequent to
650 the increase of the transpressive component.

651 For the comparison between natural data from the Austroalpine domain
652 of the Alps and the model predictions, we briefly compare the simulation
653 results with the geodynamic scenarios proposed for still active subduction
654 settings such as Cascades and Franciscan. In these contexts, the continen-
655 tal collision does not affect the subduction dynamics as in the Alps. The
656 thermal structure of the Cascades is not so different with respect to the sim-
657 ulated scenario: indeed, if we refer to fig.2 of Hyndman *et al.* (2005), notable
658 similarities between the two models can be found. In the Cascades a cold
659 fore-arc and thermal erosion of the continental lithosphere beneath the back-
660 arc region are present. The same thermal structure is also predicted by our
661 model, with a cold fore-arc region almost 100 km wide and the rising of the
662 1400 K isotherm up to 50 km depth beneath the back-arc region, accounting
663 for a high thermal regime. As a consequence, we do not expect differences
664 concerning the exhumation mechanisms but a warmer exhumation-related
665 $P-T$ evolutions would be consequent to the shallower position of the 1600K
666 isotherm (asthenosphere-lithosphere boundary). Another major difference
667 between the two models is the larger extension of the back-arc region in the

668 Cascades. This could be related to the longer subduction activity of the
669 Cascades (180-160 Ma) with respect to 65 Ma in our model (Currie *et al.*,
670 2008), that implies a continuous thermal erosion of the continental upper
671 plate. Furthermore, the higher subduction dip of the Cascades (medium and
672 deep dips: Lallemand *et al.*, 2005; Cruciani *et al.*, 2005; Currie *et al.*, 2008)
673 with respect to the presented model, would induce a larger back-arc hot re-
674 gion due to a very efficient convective cell beneath the upper plate (Currie
675 *et al.*, 2008; Roda *et al.*, 2010, 2011). The ridge very close to the trench in
676 the Cascades scenario (Hyndeman, 1995; Flueh *et al.*, 1998) also implies a
677 different thermal state with respect to that obtained by our model. Finally,
678 the oblique subduction that characterizes large part of the Cascades could
679 generate a perturbed thermal regime within the subduction zone (Thompson
680 *et al.*, 1997a,b; Rondenay *et al.*, 2008).

681 Although an early intra-oceanic subduction scenario is invoked for the
682 Franciscan compared with the ocean-continent setting adopted in our simu-
683 lations, a lot of similarities between natural and simulated data are recogniz-
684 able: (i) a wide range of peak metamorphic ages recorded by the exhumed
685 rocks (Wakabayashi & Dumitru, 2007); (ii) different P - T evolutions resulting
686 from different tectonic trajectories during subduction and exhumation, with
687 the consequent accretion of different tectono-metamorphic units at different
688 times in the same subduction zone (Wakabayashi & Dumitru, 2007); (iii)
689 the record of multiple (2 or 3) burial-exhumation cycles of blue-schist rocks
690 within 65 Ma of active subduction (Wakabayashi, 2011), although these rocks
691 have been related in the past to an accretionary wedge / subduction chan-
692 nel mechanism rather than to a hydrated mantle wedge dynamics (Cloos &

693 Shreve, 1988); (iv) the presence of *HP-HT* metamorphic rocks, which show
694 anti-clockwise *P-T-t* paths likely related to the earliest steps of the subduc-
695 tion zone (Smart & Wakabayashi, 2009) that are coherent with the predicted
696 *P-T-t* of Fig. 6; (v) prograde eclogitization of a relatively cold subducting
697 slab, and subsequent exhumation and blueschist-facies recrystallization of
698 *HP* rocks characterized by exhumation rates of several mm/a, as suggested
699 by the numerical results (Roda *et al.*, 2010; Roda, 2011).

700 CONCLUSIONS

701 The general very good agreement between the predictions of the model and
702 the natural data obtained for the Austroalpine of the Western Alps suggests
703 that the ablation of the upper plate lithosphere coupled with the dynamics
704 of the hydrated mantle wedge is a valid pre-collisional mechanism that can
705 reproduce the natural burial and exhumation evolution of this portion of the
706 Austroalpine domain during active subduction. Although this model appears
707 to be less compatible with the natural data of the Central-Eastern Alps,
708 a variation of the oceanic and/or upper plate thickness along the Ligure-
709 Piemontese ocean, a variation of the subduction rate and/or the slab dip,
710 the initial thermal state of the passive margin, the occurrence of continental
711 collision or an oblique subduction could justify a variation in the thermal
712 state from east to west along the Alpine convergent margin. Furthermore,
713 the simulated ocean-continent dynamics allows the formation of a metamor-
714 phic complex composed of juxtaposed of rocks with different metamorphic
715 evolutions, likely with a homogeneous lithostratigraphic setting, accreted in
716 the mantle wedge and exhumed during active subduction. To evaluate the

717 compatibility between natural data and the thermo-mechanical configuration
718 generated by alternative models, such as micro-continent collision (Rosen-
719 baum & Lister, 2005) and intra-continental subduction (Thöni, 2006; Janak
720 *et al.*, 2009), numerical simulations of these models could be performed in
721 the future using the same approach.

722 **ACKNOWLEDGEMENTS**

723 We would like to thank the anonymous reviewers for their constructive crit-
724 icism of the text and in particular Richard White for his accurate editorial
725 work that greatly improved the final version. Prin 2008 “Tectonic trajec-
726 tories of subducted lithosphere in the Alpine collisional orogen from struc-
727 ture, metamorphism and lithostratigraphy”, CNR-IDPA and PUR 2008 “La
728 ricerca geofisica: esplorazione, monitoraggio, elaborazione e modellazione”
729 are gratefully acknowledged. Many thanks to American Journal Experts for
730 the English revision.

731 **References**

- 732 Andreoli, M., Compagnoni, R. & Lombardo, B., 1976. Jadeite megablasts
733 from Valchiusella (Sesia-Lanzo zone, Western Alps), *Rendiconti della So-*
734 *cietà Italiana di Mineralogia e Petrologia*, **32**, 681–698.
- 735 Ayrton, S., Bugnon, C., Haarpainter, T., Weidmann, M. & Frank, E., 1982.
736 Geologie du front de la nappe de la Dent Blanche dans la region des Monts-
737 Dolins, Valais, *Eclogae Geologicae Helvetiae*, **75**, 269–286.
- 738 Babist, J., Handy, M. R., Konrad-Schmolke, M. & Hammerschmidt, K., 2006.

- 739 Precollisional, multistage exhumation of subducted continental crust: The
740 Sesia Zone, western Alps, *Tectonics*, **25**, 1–25.
- 741 Bachmann, R., Glodny, J., Oncken, O. & Seifert, W., 2009. Abandonment
742 of the South Penninic–Austroalpine palaeosubduction zone, Central Alps,
743 and shift from subduction erosion to accretion: constraints from Rb/Sr
744 geochronology, *Journal of the Geological Society*, **166**, 217–231.
- 745 Beltrando, M., Compagnoni, R. & Lombardo, B., 2010. (Ultra-) High-
746 pressure metamorphism and orogenesis: An Alpine perspective, *Gondwana*
747 *Research*, **18**, 147–166.
- 748 Best, M. G. & Christiansen, E. H., 2001., *Igneous Petrology*, Blackwell Sci.,
749 London.
- 750 Blanco-Quintero, I. F., García-Casco, A. & Gerya, T. V., 2011. Tectonic
751 blocks in serpentinite mélangé (eastern Cuba) reveal large-scale convective
752 flow of the subduction channel, *Geology*, **39**, 79–82.
- 753 Bousquet, R., 2008. Metamorphic heterogeneities within a single HP unit:
754 Overprint effect or metamorphic mix?, *Lithos*, **103**, 46–69.
- 755 Bousquet, R., Engi, M., Gosso, G., Oberhänsli, R., Berger, A., Spalla, M. I.,
756 Zucali, M. & Goffè, B., 2004. Explanatory notes to the map: metamorphic
757 structure of the Alps transition from the Western to the Central Alps,
758 *Mitt. Österr. Miner. Ges.*, **149**, 145–156.
- 759 Brun, J.-P. & Faccenna, C., 2008., Exhumation of high-pressure rocks driven
760 by slab rollback, *Earth and Planetary Science Letters*, **272**, 1–7.

- 761 Castelli, D., 1991. Eclogitic metamorphism in carbonate rocks: the example
762 of impure marbles from the Sesia - Lanzo Zone, Italian Western Alps,
763 *Journal of Metamorphic Geology*, **9**, 61–77.
- 764 Castelli, D. & Rubatto, D., 2002. Stability of Al- and F-rich titanite in
765 metacarbonate: petrologic and isotopic constraints from a polymetamor-
766 phic eclogitic marble of the internal Sesia Zone (Western Alps), *Contrib.*
767 *Mineral. Petrol.*, **142**, 627–639.
- 768 Castelli, D., Gosso, G., Rossetti, P., Spalla, M. I., Zanoni, D. & Zucali, M.,
769 2007. Guide-book to the DRT 2007 Workshop Field Excursion on the sub-
770 ducted continental crust of the Sesia-Lanzo Zone (Monte Camino-Monte
771 Mucrone; Oropa-Biella, Western Italian Alps), in *XVI DRT programs and*
772 *field guides of Conference, pre-Conference Excursion and post-Conference*
773 *Workshop*, **9**, edited by G. Gosso, A. M. Marotta, R. Sabadini & M. I.
774 Spalla, pp. 35–70, Quaderni di Geodinamica Alpina e Quaternaria, Mi-
775 lano.
- 776 Cenko-Tok, B., Oliot, E., Rubatto, D., Berger, A., Engi, M., Janots, E.,
777 Thomsen, T., Manzotti, P., Regis, D., Spandler, C., Robyr, M., &
778 Goncalves, P., 2011. Preservation of permian allanite within an alpine
779 eclogite facies shear zone at mt mucrone, italy: Mechanical and chemi-
780 cal behavior of allanite during mylonitization, *Lithos*, **125**, 40–50.
- 781 Chemenda, A. I., Mattauer, M., Malavieille, J. & Bokun, A. N., 1995.
782 A mechanism for syn-collisional rock exhumation and associated normal
783 faulting: Results from physical modelling, *Earth and Planetary Science*
784 *Letters*, **132**, 225–232.

- 785 Chopra, P. N. & Peterson, M. S., 1981. The experimental deformation of
786 dunite, *Tectonophysics*, **78**, 453–473.
- 787 Christensen, U. R., 1992. An Eulerian Technique for thermo-mechanical model
788 of lithospheric extension, *Journal of Geophysical Research*, **97**, 2015–2036.
- 789 Clift, P. & Vannucchi, P., 2004. Control on tectonic accretion versus ero-
790 sion in subduction zones: implication for the origin and recycling of the
791 continental crust., *Review of Geophysics*, **42**, 1–31.
- 792 Cloos, M., 1982. Flow melanges: numerical modelling and geo- logical con-
793 straints on their origin in the Franciscan subduction complex, *Geol. Soc.*
794 *Am. Bull.*, **93**, 330–345.
- 795 Cloos, M., 1993. Lithospheric buoyancy and collisional orogenesis: Subduc-
796 tion of oceanic plateaus, continental margins, island arcs, spreading ridges
797 and seamounts, *Geological Society of America Bulletin*, **105**, 715–737.
- 798 Cloos, M. & Shreve, R. L., 1988. Subduction-channel model of prism accre-
799 tion, melange formation, sediment subduction, and subduction erosion at
800 convergent plate margins: 2. implication and discussion, *PaGeoph.*, **128**,
801 501–545.
- 802 Compagnoni, R., 1977. The Sesia-Lanzo zone: high-pressure low-temperature
803 metamorphism in the Austroalpine continental margin, *Rendiconti della*
804 *Società Italiana di Mineralogia e Petrologia*, **33**, 335–374.
- 805 Cortiana, G. Dal Piaz, G. V. Del Moro, A. & Hunziker, J. C., 1998. 40Ar-
806 39Ar and Rb-Sr dating of the Pilonet klippe and Sesia-Lanzo basal slice in

- 807 the Ayas valley and evolution of the Austroalpine-Piedmont nappe stack,
808 *Memorie Scienze Geologiche*, **50**, 177–194.
- 809 Cosca, M. A., Sharp, Z. D. & Hunziker, J. C., 1994. Thermal and tectonic
810 evolution of the Dent Blanche nappe (Swiss and Italian Alps), in *8th In-*
811 *ternational Conference on Geochronology, Cosmochronology and Isotope*
812 *Geology (ICOG8), Berkley*, **1107**, p. 68.
- 813 Cruciani, C., Carminati, E. & Doglioni, C., 2005. Slab dip vs. lithosphere age:
814 No direct function. *Earth and Planetary Science Letters*, **238**, 298–310.
- 815 Currie, C. A., Huisman, R. S & Beaumont, C. 2008. Thinning of continental
816 backarc lithosphere by flow- induced gravitational instability, in *Earth and*
817 *Planetary Science Letters*, **269**, 436–447.
- 818 Dal Piaz, G. V., Lombardo, B. & Gosso, G., 1983. Metamorphic evolution
819 of the Mt. Emilius klippe, Dent Blanche nappe, Western Alps, *American*
820 *Journal of Science*, **283A**, 438–458.
- 821 Dal Piaz, G. V., 2001. History of tectonic interpretations of the Alps, *Journal*
822 *of Geodynamics*, **32**, 99–114.
- 823 Dal Piaz, G., Bistacchi, A. & Massironi, M., 2003. Geological outline of the
824 Alps, *Episodes*, **26**, 175–180.
- 825 Dal Piaz, G., Cortiana, G. Del Moro, A., Martin, S., Pennacchioni, G. &
826 Tartarotti, P., 2001. Tertiary age and paleostructural inferences of the
827 eclogitic imprint in the Austroalpine outliers and Zermatt-Saas ophiolite,
828 Western Alps, *Int J Earth Sci (Geol Rundsch)*, **90**, 668–684.

- 829 Dallmeyer, R. D., Neubauer, F., Handler, R., Fritz, H., Muller, W., Pana,
830 D. & Putis, M., 1996. Tectonothermal evolution of the internal Alps and
831 Carpathians: Evidence from Ar-40/Ar-39 mineral and whole-rock data,
832 *Eclogae Geologicae Helvetiae*, **89**, 203–227.
- 833 Dallmeyer, R. D., Koller, F. & Massonne, H.-J., 1997. P -T-t history of the
834 Lower Austroalpine Nappe Complex in the “Tarntaler Berge” NW of the
835 Tauern Window: implications for the geotectonic evolution of the central
836 Eastern Alps, *Contributions to Mineralogy and Petrology*, **129**, 1–19.
- 837 Delleani, F., Castelli, D., Spalla, M. I. & Gosso, G., 2010. The record of
838 subduction-related deformation in the Mt. Mucrone metagranitoids (Sesia-
839 Lanzo Zone, Western Alps), *Rend. online Soc. Geol. It.*, **10**, 46–49.
- 840 Desmons, J. & Ghent, E. D., 1977. Chemistry, zonation and distribution
841 coefficients of elements in eclogitic minerals from the eastern Sesia unit,
842 Italian Western Alps, *Schweiz. Mineral. Petrogr. Mitt.*, **57**, 397–411.
- 843 Dubois, J. & Diament, M., 1997. *Géophysique*, Masson, Paris.
- 844 Duchêne, S., J. M. Lardeaux & F. Albarede (1997), Exhumation of eclogites:
845 insights from depth-time path analysis, *Tectonophysics*, **280**, 125–140.
- 846 Engi, M., Berger, A. & Roselle, G. T., 2001. Role of the tectonic accretion
847 channel in collisional orogeny, *Geology*, **29**, 1143–1146.
- 848 Ernst, W. & Liou, J., 2008., High- and ultrahigh-pressure metamorphism:
849 Past results and future prospects, *American Mineralogist*, **93**, 1771–1786.

- 850 Ernst, W. G., Maruyama, S. & Wallis, S., 1997. Buoyancy-driven, rapid
851 exhumation of ultrahigh-pressure metamorphosed continental crust, *Proc.*
852 *Natl. Acad. Sci.*, **94**, 9532–9537.
- 853 Faccenda, M., Gerya, T. V. & Chakraborty, S., 2008. Styles of post-
854 subduction collisional orogeny: Influence of convergence velocity, crustal
855 rheology and radiogenic heat production, *Lithos*, **103**, 257–287.
- 856 Faryad, S. & Hoinkes, G., 2003. P-t gradient of eo-alpine metamorphism
857 within the austroalpine basement units east of the tauern window (austria),
858 *Mineralogy and Petrology*, **77**, 129–159.
- 859 Flueh, E. R., Fisher, M. A., Bialas, J., Childs, J. R., Klaeschen, D.,
860 Kukowski, N., Parsons, T., Scholl, D. W., ten Brink, U., Trehu, A. M.
861 & Vidal, N., 1998. New seismic images of the Cascadia subduction zone
862 from cruise SO108, *Tectonophysics*, **293**, 69–84.
- 863 Frey, M., Hunziker, J. C., Frank, W., Bocquet, J. Dal Piaz, G. V., Jager, E.
864 & Niggli, E., 1974. Alpine metamorphism of the Alps. A review, *Schweiz.*
865 *Mineral. Petrogr. Mitt.*, **54**, 247–290.
- 866 Froitzheim, N., Schmid, S. M. & Conti, P., 1994. Repeated change from
867 crustal shortening to orogen-parallel extension in the Austroalpine units
868 of Graubuenden, *Eclogae Geologicae Helvetiae*, **87**, 556–612.
- 869 Gaidies, F., Krenn, E. De Capitani, C. & Abart, R., 2008a. Coupling forward
870 modelling of garnet growth with monazite geochronology: an application
871 to the Rappold Complex (Austroalpine crystalline basement), *Journal of*
872 *Metamorphic Geology*, **26**, 775–793.

- 873 Gaidies, F., de Capitani, C., Abart, R. & Schuster, R., 2008b. Prograde
874 garnet growth along complex P–T–t paths: results from numerical exper-
875 iments on polyphase garnet from the Wolz Complex (Austroalpine base-
876 ment), *Contrib Mineral Petrol*, **155**, 673–688.
- 877 Gardien, V., Reusser, E. & Marquer, D., 1994. Pre-Alpine metamorphic
878 evolution of the gneisses from the Valpelline series (Western Alps, Italy),
879 *Schweiz. Mineral. Petrogr. Mitt.*, **74**, 489–502.
- 880 Gazzola, D., Gosso, G., Pulcrano, E. & Spalla, M. I., 2000. Eo-Alpine HP
881 metamorphism in the Permian intrusives from the steep belt of the central
882 Alps (Languard-Campo nappe and Tonale Series), *Geodinamica Acta*, **13**,
883 149–167.
- 884 Gerya, T. V. & Stockhert, B., 2002., Exhumation rates of high pressure meta-
885 morphic rocks in subduction channels: The effect of rheology., *Geophysical*
886 *Research Letters*, **29**, 1–19.
- 887 Gerya, T. V. & Stöckhert, B., 2005. Two-dimensional numerical modeling
888 of tectonic and metamorphic histories at active continental margins, *Int J*
889 *Earth Sci (Geol Rundsch)*, **95**, 250–274.
- 890 Gerya, T. V., Perchuk, L. L. & Burg, J. P., 2008. Transient hot channels: Per-
891 petrating and regurgitating ultrahigh-pressure, high-temperature crust–
892 mantle associations in collision belts, *Lithos*, **103**, 236–256.
- 893 Giorgetti, G., Tropper, P., Essene, E. J. & Peacor, D. R., 2000. Char-
894 acterization of non-equilibrium and equilibrium occurrences of parago-

- 895 nite/muscovite intergrowths in an eclogite from the Sesia±Lanzo Zone
896 (Western Alps, Italy), *Contrib Mineral Petrol*, **138**, 326–336.
- 897 Gosso, G., Kienast, J. R., Lardeaux, J. M. & Lombardo, B., 1982. Replisse-
898 ment intense et transposition (en climat métamorphique de haute pres-
899 sion) fes contacts tectoniques majeurs dans l'edifice supérieur des nappes
900 alpines (zone Sesia-Lanzo), *Compte Rendu Academie des Sciences Paris*,
901 **294**, 343–348.
- 902 Gosso, G., Messiga, B., Rebay, G. & Spalla, M. I., 2010., The interplay
903 between deformation and metamorphism during eclogitization of amphi-
904 bolites in the Sesia-Lanzo zone of the Western Alps, *International Geology*
905 *Review*, **51**, 1193–1219.
- 906 Gregurek, D., Abart, R. & Hoinkes, G., 1997. Contrasting eoalpine p-t evolu-
907 tions in the southern koralpe, eastern alps, *Mineralogy and Petrology*, **60**,
908 61–80.
- 909 Groppo, C., Beltrando, M. & Compagnoni, R., 2009. The PT path of the
910 ultra-high pressure Lago Di Cignana and adjoining high-pressure meta-
911 ophiolitic units: insights into the evolution of the subducting Tethyan
912 slab, *Journal of Metamorphic Geology*, **27**, 207–231.
- 913 Guillot, S., Hattori, K., Agard, P., Schwartz, S. & Vidal, O., 2009. Ex-
914 humation Processes in Oceanic and Continental Subduction Contexts: A
915 Review, in *Subduction Zone Dynamics*. edited by S. Lallemand & F. Fu-
916 niciello, pp. 175–204, Springer-Verlag Berlin Heidelberg.

- 917 Guntli, P. & Liniger, M., 1989. Metamorphose in der Margna-Decke im Bere-
918 ich Piz de la Margna und Piz Fedoz (Oberengadin), *Schweiz. Mineral.*
919 *Petrogr. Mitt.*, **69**, 289–301.
- 920 Habler, G., Linner, M., Thiede, R. & Thöni, M., 2001. The P-T-t-D Evolu-
921 tion of the Cretaceous Metamorphism in the Central Schneeberg Complex
922 (Eastern Alps, Italy/Austria): Andalusite-formation during decompres-
923 sion, *Geol. Paläont. Mitt. Innsbruck*, **25**, 107–109.
- 924 Habler, G., Thöni, M. & Sölva, H., 2006. Tracing the high pressure stage in
925 the polymetamorphic Texel Complex (Austroalpine basement unit, East-
926 ern Alps):P-T-t-d constraints, *Mineralogy and Petrology*, **88**, 269–296.
- 927 Haenel, R., Rybach, L. & Stegena, L., 1988. *Handbook of Terrestrial Heat-*
928 *Flow Density Determination*, Kluwer Academic Publishers.
- 929 Handy, M., Herwegh, M., Kamber, B., Tietz, R. & Villa, I., 1996. Geochrono-
930 logic, petrologic and kinematic constraints on the evolution of the err-
931 platta boundary, part of a fossil continent-ocean suture in the alps (east-
932 ern switzerland), *Schweizerische Mineralogische Und Petrographische Mit-*
933 *teilungen*, **76**, 453–474.
- 934 Handy, M. R. & Oberhänsli, R., 2004. Explanatory notes to the map: meta-
935 morphic structure of the Alps age map of the metamorphic structure of
936 the Alps - tectonic interpretation and outstanding problem, *Mitt. Österr.*
937 *Miner. Ges.*, **149**, 201–225.
- 938 Handy, M. R., Schmid, S. M., Bousquet, R., Kissling, E. & Bernoulli, D.,
939 2010. Reconciling plate-tectonic reconstructions of Alpine Tethys with the

- 940 geological–geophysical record of spreading and subduction in the Alps,
941 *Earth-Science Reviews*, **102**, 121–158.
- 942 Hellwig, D., 2003. Die mobilisierung der austroalpinen Dent Blanche decke
943 auf fluid-induzierten scherzonen während alpiner hochdruckmetamorphose,
944 Ph.D. thesis, Fachbereich Geowissenschaften der Philipps-Universität Mar-
945 burg.
- 946 Hoinkes, G., Kostner, A. & Thöni, M., 1991. Petrologic constraints for
947 Eoalpine eclogite Facies Metamorphism in the Austroalpine Oetztal Base-
948 ment, *Mineralogy and Petrology*, **43**, 237–254.
- 949 Hopfer, N., 1995. Sedimentäre Abfolge und Alpine Überprägung der Per-
950 motriassischen Roisan Zone (Südliche Austroalpine Dent Blanche Decke,
951 Italienische Westalpen), Ph.D. thesis, Philipps-Universität Marburg.
- 952 Hunziker, J. C., 1974. Rb/Sr and K/Ar age determination and the Alpine
953 tectonic history of the Western Alps, *Memorie degli Istituti di Geologia e*
954 *Mineralogia dell’Università di Padova*, **31**, 1–54.
- 955 Hunziker, J. C., Desmons, J. & Hurford, A. J., 1992. Thirty-two years of
956 geochronological work in the Central and Western Alps: a review of seven
957 maps, *Mem. Geol. Lausanne*, **13**, 1–59.
- 958 Hy, C., 1984. Métamorphisme polyphasé et évolution tectonique dans la
959 croûte continentale écoligisée: les séries granitiques et pélitiques du Monte
960 Mucrone (zone Sesia- Lanzo, Alpes italiennes), Ph.D. thesis, Paris VI.

- 961 Hyndeman, R. D., 1995. The lithoprobe corridor across the Vancouver Is-
962 land and tectonic consequences of subduction, *Canadian Journal of Earth*
963 *Sciences*, **32**, 1777–1802.
- 964 Hyndman, R. D., Fluck P., Mazzotti S., Lewis T., Ristau J. & Leonard,
965 L., 2005. Current tectonics of the northern canadian cordillera, *Canadian*
966 *Journal of Earth Sciences*, **42**, 1117–1136.
- 967 Inger, S., Ramsbotham, W., Cliff, R. A. & Rex, D. C., 1996. Metamorphic
968 evolution of the Sesia-Lanzo Zone, Western Alps: time constraints from
969 multisystem geochronology, *Contributions to Mineralogy and Petrology*,
970 **126**, 152–168.
- 971 Janak, M., Cornell, D., Froitzheim, N. De Hoog, J. C. M., Broska, I.,
972 Vrabec, M. & Hurai, V., 2009. Eclogite-hosting metapelites from the Po-
973 horje Mountains (Eastern Alps): P-T evolution, zircon geochronology and
974 tectonic implications, *European Journal of Mineralogy*, **21**, 1191–1212.
- 975 Karato, S. & Wu, P., 1987. Rheology of the Upper Mantle: A Synthesis,
976 *Science*, **260**, 771–778.
- 977 Kienast, J. R., 1983. Le métamorphisme de haute pression et basse
978 température (Eclogites et Schistes Bleus): Données nouvelles sur la
979 pétrologie de la croûte océanique subductée et des sédiments associés,
980 Ph.D. thesis, Université de Paris VI.
- 981 Kienast, J. R. & Nicot, E., 1971. Presence d'une paragenese a disthene et
982 chloritoide (d'age alpin probable) dans les gneiss a sillimanite, grenat et

- 983 cordierite de Valpelline (Val d'Aoste, Italie), *Compte Rendu Academie des*
984 *Sciences Paris*, **D 272**, 1836–1839.
- 985 Kirby, S. H., 1983. Rheology of the Lithosphere, *Review of Geophysics*, **21**,
986 1459–1487.
- 987 Koller, F., 2003. 5TH workshop of Alpine geological studies field trip guide
988 e5 low T - high P metamorphism in the Tarntal Mountains (Lower Aus-
989 trolpine Unit), *Geol. Paläont. Mitt. Innsbruck*, **26**, 47–59.
- 990 Konzett, J. & Hoinkes, G., 1996. Paragonite-hornblende assemblages and
991 their petrological significance: An example from the austroalpine schnee-
992 berg complex, southern tyrol, italy, *Journal of Metamorphic Geology*, **14**,
993 85–101.
- 994 Kurz, W. & Fritz, H., 2003. Tectonometamorphic evolution of the aus-
995 troalpine nappe complex in the central eastern alps - consequences for
996 the eo-alpine evolution of the eastern alps, *International Geology Review*,
997 **45**, 1100–1127.
- 998 Lallemand, S., Heuret, A. & Boutelier, D., 2005. On the relationships between
999 slab dip, back-arc stress, upper plate absolute motion, and crustal nature
1000 in subduction zones. *Geochemistry Geophysics Geosystems* **6**, 1–18.
- 1001 Lardeaux, J. M. & Spalla, M. I., 1991. From granulites to eclogites in the
1002 Sesia zone (Italian Western Alps): a record of the opening and closure of
1003 the Piedmont ocean, *Journal of Metamorphic Geology*, **9**, 35–59.
- 1004 Lardeaux, J. M., Gosso, G., Kienast, J. R. & Lombardo, B., 1982. Relations
1005 entre le métamorphisme et la déformation dans la zone Sésia-Lanzo (Alpes

- 1006 Occidentales) et le problème de l'éclogitisation de la croûte continentale,
1007 *Bulletin de la Société Géologique de France*, **24**, 793–800.
- 1008 Lardeaux, J. M., Lombardo, B., Gosso, G. & Kienast, J. R., 1983. Découverte
1009 de paragenèses à ferro-omphacites dans les orthogneiss de la zone Sesia-
1010 Lanzo septentrionale (Alpes Italiennes), *Compte Rendu Academie des Sci-
1011 ences Paris*, **296**, 453–456.
- 1012 Linner, M., 1999. Die P-T-t Entwicklung der Eklogite im Schoberkristallin
1013 als Beleg für frühe alpidische kontinentale Subduktion im Ostalpinen
1014 Kristallin, Ph.D. thesis, Inst of Petrology, Univ Vienna.
- 1015 Mandl, G. & Ondrejicka, G., 1993. Radiolarite und Conodonten aus dem
1016 Meliaticum im Ostabschnitt der NKA, *Jahrbuch der Geologischen Bunde-
1017 sanstalt*, **136**, 841–871.
- 1018 Marotta, A. M., Spelta, E. & Rizzetto, C., 2006. Gravity signature of crustal
1019 subduction inferred from numerical modelling, *Geophys. J. Int.*, **166**, 923–
1020 938.
- 1021 Marotta, A. M., Spalla, M. I. & Gosso, G., 2009. Upper and lower crustal
1022 evolution during lithospheric extension: numerical modelling and natural
1023 footprints from the European Alps, in *Extending a Continent: Architec-
1024 ture, Rheology and Heat Budget*, vol. 321. edited by U. Ring & B. Wernicke,
1025 pp. 33–72, The Geological Society, London, Special Publications.
- 1026 Meda, M., Marotta, A. & Spalla, M., 2010. The role of mantle hydration
1027 into the continental crust recycling in the wedge region, *Geological Society,
1028 London, Special Publications*, **332**, 149–172.

- 1029 Miller, C. & Thöni, M., 1997. Eo-alpine eclogitisation of Permian MORB-
1030 type gabbros in the Koralpe (Eastern Alps, Austria): new geochronologi-
1031 cal, geochemical and petrological data, *Chemical Geology*, **137**, 283–310.
- 1032 Neubauer, F., Dallmeyer, R. D. & Takasu, A., 1999. Conditions of eclog-
1033 ite formation and age of retrogression within the Siegraben unit, eastern
1034 Alps: implications for Alpine-Carpathian tectonics, *Schweiz. Mineral. Pet-
1035 rogr. Mitt.*, **79**, 297–307.
- 1036 Oberhänsli, R., 2004. Explanatory notes to the map: metamorphic structure
1037 of the Alps, *Mitt. Osterr. Miner. Ges.*, **149**, 1–226.
- 1038 Oberhänsli, R., Hunziker, J. C., Martinotti, G. & Stern, W. B., 1985. Geo-
1039 chemistry, geochronology and petrology of Monte Mucrone: An example
1040 of EO-alpine eclogitization of Permian granitoids in the Sesia-Lanzo Zone,
1041 Western Alps, Italy, *Chemical Geology*, **52**, 165–184.
- 1042 Pennacchioni, G., 1988. Studio geologico del tratto meridionale della dor-
1043 sale tra Valnontey e Valleile (Cogne, Valle d'Aosta), *Memorie di Scienze
1044 Geologiche*, **40**, 333–354.
- 1045 Pennacchioni, G. & Guermani, A., 1993. The mylonites of the Austroalpine
1046 Dent Blanche Nappe along the northwestern side of the Valpelline Valley
1047 (Italian Western Alps), *Memorie Scienze Geologiche*, **45**, 37–55.
- 1048 Platt, J. P., 1986. Dynamic of orogenic wedges and the uplift of high-pressure
1049 metamorphic rocks, *Geol. Soc. Am. Bull.*, **97**, 1037–1053.
- 1050 Pognante, U., 1989. Lawsonite, blueschist and eclogite formation in the

- 1051 southern Sesia Zone (Western Alps, Italy), *European Journal of Miner-*
1052 *alogy*, **1**, 89–104.
- 1053 Pognante, U., 1991. Petrological constraints on the eclogite- and blueschist-
1054 facies metamorphism and P-T-t paths in the Western Alps, *Journal of*
1055 *Metamorphic Geology*, **9**, 5–17.
- 1056 Pognante, U., Talarico, F., Rastelli, N. & Ferrati, N., 1987. High pressure
1057 metamorphism in the nappes of the Valle dell'Orco traverse (Western Alps
1058 collisional belt), *Journal of Metamorphic Geology*, **5**, 397–414.
- 1059 Poli, S., 1991. Reaction spaces and P-T paths: from the amphibole eclogite
1060 to the greenschist facies in the Austroalpine domain (Oetztal Complex),
1061 *Contributions to Mineralogy and Petrology*, **106**, 399–416.
- 1062 Polino, R. Dal Piaz, G. & Gosso, G., 1990. Tectonic erosion at the Adria
1063 margin and accretionary processes for the Cretaceous orogeny of the Alps.,
1064 *Mémoires de la Société Géologique de France*, **156**, 345–367.
- 1065 Putis, M., Korikovsky, S. & Pushkarev, Y., 2000. Petrotectonics of an Aus-
1066 troalpine eclogite-bearing complex (Sieggraben, Eastern Alps) and U-Pb
1067 dating of exhumation, *Jahrbuch Geologische Bundesanstalt*, **142**, 73–93.
- 1068 Putis, M., Korikovsky, S., Wallbrecher, E., Unzog, W., Olesen, N. & Fritz,
1069 H., 2002. Evolution of an eclogitized continental fragment in the eastern
1070 alps (sieggraben, austria), *Journal of Structural Geology*, **24**, 339–357.
- 1071 Ranalli, G. & Murphy, D. C., 1987. Rheological stratification of the litho-
1072 sphere, *Tectonophysics*, **132**, 281–295.

- 1073 Rebay, G. & Messiga, B., 2007. Prograde metamorphic evolution and de-
1074 velopment of chloritoid-bearing eclogitic assemblages in subcontinental
1075 metagabbro (Sesia-Lanzo zone, Italy), *Lithos*, **98**, 275–291.
- 1076 Rebay, G. & Spalla, M. I., 2001. Emplacement at granulite facies conditions of
1077 the Sesia-Lanzo metagabbros: an early record of Permian rifting?, *Lithos*,
1078 **58**, 85–104.
- 1079 Reinsch, D., 1979. Glaucophanites and eclogites from val chiusella, sesia-
1080 lanzo zone (italian alps), *Contributions to Mineralogy and Petrology*, **70**,
1081 257–266.
- 1082 Ring, U. & Layer, P. W., 2003. High-pressure metamorphism in the Aegean,
1083 eastern Mediterranean: Underplating and exhumation from the Late Cre-
1084 taceous until the Miocene to Recent above the retreating Hellenic subduc-
1085 tion zone, *Tectonics*, **22**, 1–23.
- 1086 Roda, M., 2011. Integration of natural data within a numerical model for the
1087 geodynamic reconstruction of an inner portion of the Alps, Ph.D. thesis,
1088 Univerisità degli Studi di Milano.
- 1089 Roda, M. & Zucali, M., 2008. Meso and microstructural evolution of the
1090 Mont Morion metaintrusive complex (Dent Blanche nappe, Austroalpine
1091 domain, Valpelline, Western Italian Alps), *Boll. Soc. Geol. It. (Ital. J.*
1092 *Geosci.)*, **127**, 105–123.
- 1093 Roda, M., Marotta, A. M. & Spalla, M. I., 2010., Numerical simulations of
1094 an ocean-continent convergent system: Influence of subduction geometry

- 1095 and mantle wedge hydration on crustal recycling, *Geochemistry Geophysics*
1096 *Geosystems*, **11**, 1–21.
- 1097 Roda, M., Marotta, A. M. & Spalla, M. I., 2011. The effects of the overrid-
1098 ing plate thermal state on the slab dip in an ocean-continent subduction
1099 system, *Compte Rendu Academie des Sciences Paris*, **343**, 323–330.
- 1100 Rolfo, F., Compagnoni, R. & Tosoni, D., 2004. Geology and petrology of
1101 the Austroalpine Chatillon slice, Aosta valley, western Alps, *Geodinamica*
1102 *Acta*, **17**, 91–105.
- 1103 Rolland, Y., Lardeaux, J. M., Guillot, S. & Nicollet, C., 2000. Extension syn-
1104 convergence, poinconnement vertical et unités métamorphiques contrastées
1105 en bordure ouest du grand paradis (alpes franco-italiennes), *Geodinamica*
1106 *Acta*, **13**, 133–148.
- 1107 Rondenay, S., Abers, G. A. & Keken, P. E. V., (2008). Seismic imaging of
1108 subduction zone metamorphism, *Geology*, **36**, 275–278.
- 1109 Rosenbaum, G. & Lister, G. S., 2005. The Western Alps from the Jurassic to
1110 Oligocene: spatio-temporal constraints and evolutionary reconstructions,
1111 *Earth-Science Reviews*, **69**, 281–306.
- 1112 Rubatto, D., 1998. Dating of pre-Alpine magmatism, Jurassic ophiolites and
1113 Alpine subductions in the western Alps, Ph.D. thesis, ETH - Zurich.
- 1114 Rubatto, D., Gebauer, D. & Compagnoni, R., 1999. Dating of eclogite-facies
1115 zircons: the age of Alpine metamorphism in the Sesia-Lanzo Zone (Western
1116 Alps), *Earth and Planetary Science Letters*, **167**, 141–158.

- 1117 Rubatto, D., Regis, D., Hermann, J., Boston, K., Engi, M., Beltrando, M. &
1118 McAlpine, S. R. B., 2011. Yo-yo subduction recorded by accessory minerals
1119 in the Italian Western Alps, *Nature Geoscience*, **4**, 338–342.
- 1120 Ruffet, G., Féraud, G., Balèvre, M. & Kiénast, J.-R., 1995. Plateau ages
1121 and excess argon in phengites: an ^{40}Ar — ^{39}Ar laser probe study of Alpine
1122 micas (Sesia Zone, Western Alps, northern Italy), *Chemical Geology*, **121**,
1123 327–343.
- 1124 Scambelluri, M., Pennacchioni, G. & Philippot, P., 1998. Salt-rich aqueous
1125 fluids formed during eclogitization of metabasites in the Alpine continental
1126 crust (Austroalpine Mt. Emilius unit, Italian western Alps), *Lithos*, **43**,
1127 151–167.
- 1128 Schmid, S. M., Fügenschuh, B., Kissling, E. & Schuster, R., 2004. Tectonic
1129 map and overall architecture of the alpine orogen, *Eclogae Geologicae Hel-*
1130 *vetiae*, **97**, 93–117.
- 1131 Schneider, J., Bosch, D., Monie, P., Guillot, S., Garcia-Casco, A., Lardeaux,
1132 J. M., MarteTorres-Roldan, R. L. & Trujillo, G. M., 2004. 3-d modelling
1133 of alpine mohos in southwestern alps, *Geophysical Journal International*,
1134 **180**, 961–975.
- 1135 Schreiber, D., Lardeaux, J. M., Martelet, G., Courrioux, G. & Guillen A.,
1136 2010. Origin and evolution of the Escambray Massif (Central Cuba): an
1137 example of HP/LT rocks exhumed during intraoceanic subduction, *Journal*
1138 *of Metamorphic Geology*, **22**, 227–247.

- 1139 Schuster, R. & Frank, W., 1999. Metamorphic evolution of the Austroalpine
1140 units east of the Tauern Window: indications for Jurassic strike slip tec-
1141 tonics, *Mitt. Ges. Geol. Bergbaustud. Osterr.*, **42**, 37–58.
- 1142 Schuster, R., Scharbert, S., Abart, R. & Frank, W., 2001. Permo-Triassic
1143 extension and related HT/ LP metamorphism in the Austroalpine-
1144 Southalpine realm, *Mitt. Ges. Geol. Bergbaustud. Oesterr.*, **45**, 111–141.
- 1145 Schuster, R., Koller, F., Hoeck, V., Hoinkes, G., & Bousquet, R., 2004.
1146 Explanatory notes to the map: metamorphic structure of the Alps age
1147 map of the metamorphic structure of the Alps - metamorphic evolution of
1148 the Eastern Alps, *Mitt. Osterr. Miner. Ges.*, **149**, 175–199.
- 1149 Schwartz, S., Lardeaux, J. M., Guillot, S., & Tricart, P., 2000. Diversité du
1150 métamorphisme éclogitique dans le massif ophiolitique du Monviso (Alpes
1151 Occidentales, Italie), *Geodinamica Acta*, **13**, 169–188.
- 1152 Schwartz, S., Lardeaux, J. M., Tricart, P., Guillot, S., & Labrin, E., 2007.
1153 Diachronous exhumation of hp-lt metamorphic rocks from south-western
1154 alps: evidence from fission-track analysis, *Terra Nova*, **19**, 133–140.
- 1155 Shreve, R. L. & Cloos, M., 1986. Dynamics of sediment subduction, melange
1156 formation and prism accretion, *Journal of Geophysical Research*, **91**,
1157 10229–10245.
- 1158 Smart, C. M. & Wakabayashi, J., 2009. Hot and deep: Rock record of subduc-
1159 tion initiation and exhumation of high-temperature, high-pressure meta-
1160 morphic rocks, feather river ultramafic belt, california, *Lithos*, **113**, 292–
1161 305.

- 1162 Solva, H., Thoni, M., Grasemann, B. & Linner, M., 2001. Emplacement of eo-
1163 alpine high-pressure rocks in the austroalpine otztal complex (texel group,
1164 italy/austria), *Geodinamica Acta*, **14**, 345–360.
- 1165 Solva, H., Grasemann, B., Thoni, M., Thiede, R. & Habler, G., 2005. The
1166 schneeberg normal fault zone: Normal faulting associated with cretaceous
1167 se-directed extrusion in the eastern alps (italy/austria), *Tectonophysics*,
1168 **401**, 143–166.
- 1169 Spalla, M. I., 1993. Microstructural control on the P-T path construction
1170 in metapelites of the Austroalpine crust (Texel Gruppe, Eastern Alps),
1171 *Schweizerische Mineralogische Und Petrographische Mitteilungen*, **81**, 197–
1172 212.
- 1173 Spalla, M. I., Messiga, B. & Gosso, G., 1995. LT-Alpine overprint on the HT
1174 rifting-related metamorphism in the steep belt of the Languard-Campo
1175 Nappe. The Cima Rovaia and Scisti del Tonale Units represent two differ-
1176 ent extents of Alpine re-equilibration, in *International Ophiolite Sympo-*
1177 *sium*, p. 148.
- 1178 Spalla, M., Lardeaux, J. Dal Piaz, G., Gosso, G. & Messiga, B., 1996. Tec-
1179 tonic significance of the Alpine eclogites, *Journal of Geodynamics*, **21**,
1180 257–285.
- 1181 Spalla, M. I., Messiga, B. & Gosso, G., 1997. Deeper tectonic trajectories for
1182 some Sesia-Lanzo zone metabasites, *Quad. Geod. Alp. Quat.*, **4**, 123–124.
- 1183 Spalla, M. I., Zucali, M., Di Paola, S. & Gosso, G. 2005. A critical assessment
1184 of the tectono-thermal memory of rocks and definition of the tectonomet-

- 1185 morphic units: evidence from fabric and degree of metamorphic transfor-
1186 mations, *Geol. Soc. Spe. Pub.*, **243**, 227–247.
- 1187 Spalla, M. I., Gosso, G., Marotta, A. M., Zucali, M. & Salvi, F., 2010.
1188 Analysis of natural tectonic systems coupled with numerical modelling of
1189 the polycyclic continental lithosphere of the Alps, *International Geology*
1190 *Review*, **52**, 1268–1302.
- 1191 Stöckhert, B., Jager, E. & Voll, G., 1986. K-Ar age determinations on phen-
1192 gites from the internal part of the Sesia zone, lower Aosta Valley (Western
1193 Alps, Italy), *Contributions to Mineralogy and Petrology*, **92**, 456–470.
- 1194 Stüwe, K. & Powell, R., 1995. PT Paths from modal proportions: application
1195 to the Koralm Complex, Eastern Alps, *Contributions to Mineralogy and*
1196 *Petrology*, **119**, 83–93.
- 1197 Stüwe, K. & Schuster, R., 2010. Initiation of subduction in the Alps: Conti-
1198 nent or ocean?, *Geology*, **38**, 175–178.
- 1199 Tenczer, V. & Stüwe, K., 2003. The metamorphic field gradient in the eclog-
1200 ite type locality, Koralpe region, Eastern Alps, *Journal of Metamorphic*
1201 *Geology*, **21**, 377–393.
- 1202 Tenczer, V., Powell, R. & Stüwe, K., 2006. Evolution of H₂O content in a
1203 polymetamorphic terrane: the Plattengneiss Shear Zone (Koralpe, Aus-
1204 tria), *Journal of Metamorphic Geology*, **24**, 281–295.
- 1205 Thompson, A. B., Schulmann, K. & Jezek, J., 1997a. Thermal evolution

- 1206 and exhumation in obliquely convergent (transpressive) orogens, *Tectono-*
1207 *physics*, **280**, 171–184.
- 1208 Thompson, A. B., Schulmann, K. & Jezek, J., 1997b. Extrusion tectonics
1209 and elevation of lower crustal metamorphic rocks in convergent orogens,
1210 *Geology*, **25**, 491–494.
- 1211 Thöni, M., 2006. Dating eclogite-facies metamorphism in the eastern alps –
1212 approaches, results, interpretations: a review, *Mineralogy and Petrology*,
1213 **88**, 123–148.
- 1214 Thöni, M. & Miller, C. H., 1996. Garnet Sm–Nd data from the Saualpe and
1215 the Koralpe (Eastern Alps, Austria): chronological and P–T constraints
1216 on the thermal and tectonic history, *Journal of Metamorphic Geology*, **14**,
1217 453–466.
- 1218 Thöni, M., Miller, C. Blichert-toft, J., Whitehouse, M. J., Konzett, J. &
1219 Zanetti, A., 2008. Timing of high-pressure metamorphism and exhumation
1220 of the eclogite type-locality (Kupplerbrunn–Prickler Halt, Saualpe, south-
1221 eastern Austria): constraints from correlations of the Sm–Nd, Lu–Hf, U–
1222 Pb and Rb–Sr isotopic systems, *Journal of Metamorphic Geology*, **26**, 561–
1223 581.
- 1224 Tomaschek, F. & Blümel, P., 1998. Eo-Alpine medium grade metamorphism
1225 in the Austroalpine Campo basement at Passo di Gavia (northern Italian
1226 Alps), *Terra Nostra*, **98**, 78–79.
- 1227 Torok, K., 1999. Alpine P-T and Fluid Evolution of Micaschists from the
1228 Sopron Area (E-Alps, W-Hungary), *Terra Abstract*, **11**, 791.

- 1229 Torok, K., 2003. Alpine P-T path of micaschists and related orthogneiss veins
1230 near Óbrennberg (W-Hungary, Eastern Alps), *N. Jb. Miner. Abh.*, **179**,
1231 101–142.
- 1232 Tropper, P. & Essene, E. J., 2002. Thermobarometry in eclogites with mul-
1233 tiple stages of mineral growth: an example from the Sesia-Lanzo Zone
1234 (Western Alps, Italy), *Swiss Bulletin of Mineralogy and Petrology*, **82**,
1235 487–514.
- 1236 Tropper, P., Essene, E. J., Sharp, Z. D. & Hunziker, J. C., 1999. Applica-
1237 tion of K-feldspar- jadeite-quartz barometry to eclogite facies metagranites
1238 and metapelites in the Sesia-lanzo Zone (Western Alps, Italy), *Journal of*
1239 *Metamorphic Geology*, **17**, 195–209.
- 1240 Tropper, P., Bernhard, F. & Konzett, J., 2001. Trace Element Mobility in
1241 Contact Metamorphic Rocks: Baddeleyite-Zirconolite- (Zircon) Veins in
1242 Olivine-Bearing Marbles from the Stubenberg Granite Contact Aureole
1243 (Styria, Austria), *Journal of Conference Abstract*, **6**, 278.
- 1244 Turcotte, D. L. & Schubert, G., 2002. *Geodynamics*, 2nd ed., Cambridge
1245 University Press, New York.
- 1246 Vuichard, J. P. & Balleve, M., 1988. Garnet-chloritoid equilibria in eclogitic
1247 pelitic rocks from the Sesia zone (Western Alps): their bearing on phase
1248 relations in high pressure metapelites, *Journal of Metamorphic Geology*,
1249 **6**, 135–157.
- 1250 Wakabayashi, J., 2011. Subducted sedimentary serpentinite mélanges:

- 1251 Record of multiple burial–exhumation cycles and subduction erosion,
1252 *Tectonophysics*, **in press**.
- 1253 Wakabayashi, J., & Dumitru, T. A., 2007. Ar-40/Ar-39 ages from coherent,
1254 high-pressure metamorphic rocks of the Franciscan complex, California:
1255 Revisiting the timing of metamorphism of the world’s type subduction
1256 complex *International Geology Review*, **49**, 873–906.
- 1257 Warren, C. J., Beaumont, C. & Jamieson, R. A., 2008. Deep subduction
1258 and rapid exhumation: Role of crustal strength and strain weakening in
1259 continental subduction and ultrahigh-pressure rock exhumation, *Tectonics*,
1260 **27**, 1–28.
- 1261 Wiesinger, M., Neubauer, F. & Handler, R., 2005. Exhumation of the Saualpe
1262 eclogite unit, Eastern Alps: constraints from $^{40}\text{Ar}/^{39}\text{Ar}$ ages and struc-
1263 tural investigations, in *Geophysical Research Abstracts*, vol. 7. edited by
1264 E. G. Union, p. 05066.
- 1265 Williams, P. F. & Compagnoni, R., 1983. Deformation and metamorphism in
1266 the Bard area of the Sesia Lanzo Zone, Western Alps, during subduction
1267 and uplift, *Journal of Metamorphic Geology*, **1**, 117–140.
- 1268 Yamato, P., Agard, P., Burov, E., Pourhiet, L. L., Jolivet, L. & Tiberi, C.,
1269 2007. Burial and exhumation in a subduction wedge: Mutual constraints
1270 from thermomechanical modeling and natural P-T-t data (Schistes Lustrés,
1271 western Alps), *Journal of Geophysical Research*, **112**, 1–28.
- 1272 Zanchetta, S., 2007. Evoluzione tettonometamorica delle unità di Texel e
1273 dello Schneeberg (Alpi centro-orientali), *Rend. Soc. Geol. It.*, **4**, 312–314.

- 1274 Zanoni, D., 2010. Structural and petrographic analysis at the north-eastern
1275 margin of the Oligocene Traversella pluton (Internal Western Alps, Italy),
1276 *Italian Journal of Geosciences*, **129**, 51–68.
- 1277 Zanoni, D., Bado, L., Spalla, M., Zucali, M. & Gosso, G., 2008. Structural
1278 analysis of the northeastern margin of the tertiary intrusive stock of Biella
1279 (Western Alps, Italy), *Boll. Soc. Geol. It. (Ital. J. Geosci.)*, **127**, 125–140.
- 1280 Zanoni, D., Spalla, M. I. & Gosso, G., 2010. Structure and PT estimates
1281 across late-collisional plutons: constraints on the exhumation of western
1282 Alpine continental HP units, *International Geology Review*, **52**, 1244–1267.
- 1283 Zucali, M. & Spalla, M. I., 2011. Prograde lawsonite during the flow of con-
1284 tinental crust in the Alpine subduction: Strain vs. metamorphism parti-
1285 tioning, a field-analysis approach to infer 5 tectonometamorphic evolutions
1286 (Sesia-Lanzo Zone, Western Italian Alps), *Journal of Structural Geology*,
1287 **33**, 381–398.
- 1288 Zucali, M., Spalla, I. & Gosso, G., 2002. Strain partitioning and fabric evo-
1289 lution as a correlation tool: the example of the Eclogitic Micaschists Com-
1290 plex in the Sesia-Lanzo Zone (Monte Mucrone-Monte Mars, Western Alps,
1291 Italy), *Schweiz. Mineral. Petrogr. Mitt.*, **82**, 429–454.
- 1292 Zucali, M., Spalla, M., Gosso, G., Racchetti, S. & Zulbati, F., 2004. Prograde
1293 LWS-KY transition during subduction of the Alpine continental crust of
1294 the Sesia- Lanzo Zone: The Ivizio Complex, *Journal of the Virtual Ex-
1295 plorer, Electronic Edition*, **16**, 1–21.

1296 **FIGURE CAPTIONS**

1297 Fig. 1: Locations from which natural data were obtained within the Aus-
1298 troalpine Domain upon the structural map of the Alps, redrawn after Schmid
1299 *et al.* (2004), (Thöni, 2006) and Castelli *et al.* (2007). Western Alps (a).
1300 Refs. 1: Castelli (1991); 2: Vuichard & Ballevre (1988); 3: Lardeaux &
1301 Spalla (1991); 4: Castelli & Rubatto (2002); 5: Lardeaux *et al.* (1982); 6:
1302 Gosso *et al.* (1982); 7: Hy (1984); 8: Oberhänsli *et al.* (1985); 9: Compagnoni
1303 (1977); 10: Zucali *et al.* (2002); 11: Delleani *et al.* (2010); 12: Rubatto *et al.*
1304 (1999); 13: Giorgetti *et al.* (2000); 14: Tropper & Essene (2002); 15: Tropper
1305 *et al.* (1999); 16: Williams & Compagnoni (1983); 17: Spalla *et al.* (1997)
1306 and Gosso *et al.* (2010); 18: Ruffet *et al.* (1995); 19: Zucali *et al.* (2004) and
1307 Zucali & Spalla (2011); 20: Andreoli *et al.* (1976); 21: Reinsch (1979); 22:
1308 Desmons & Ghent (1977); 23: Pognante (1989); 24: Pognante *et al.* (1987);
1309 25: Rebay & Messiga (2007) and Lardeaux & Spalla (1991); 26: Pognante
1310 (1989); 27: Williams & Compagnoni (1983); 28: Pognante *et al.* (1987); 29:
1311 Lardeaux *et al.* (1983); 30: Pognante *et al.* (1987); 31: Pognante (1989);
1312 32: Rolfo *et al.* (2004); 33: Hellwig (2003); 34: Roda & Zucali (2008); 35:
1313 Kienast & Nicot (1971); 36: Hopfer (1995); 37: Kienast (1983); 38: Dal Piaz
1314 *et al.* (1983); 39: Pennacchioni (1988); 40: Scambelluri *et al.* (1998); 41:
1315 Dal Piaz *et al.* (2003); 42: Cortiana *et al.* (1998); 43 and 44: Rubatto *et al.*
1316 (2011). Central Alps (b). Refs. 1: Gazzola *et al.* (2000); 2: Spalla *et al.*
1317 (1995); 3: Tomaschek & Blümel (1998); 4: Handy *et al.* (1996); 5: Guntli
1318 & Liniger (1989); 6: Konzett & Hoinkes (1996); 7: Habler *et al.* (2001); 8:
1319 Solva *et al.* (2001); 9: Spalla (1993); 10: Hoinkes *et al.* (1991); 11: Zanchetta
1320 (2007); 12: Habler *et al.* (2006). Eastern Alps (c). Refs. 1: Koller (2003); 2:

1321 Linner (1999); 3 and 4 Faryad & Hoinkes (2003); 5: Gaidies *et al.* (2008a);
1322 6: Gaidies *et al.* (2008b); 7: Thöni *et al.* (2008); 8: Thöni & Miller (1996);
1323 9: Stüwe & Powell (1995); 10, 11, 12 and 13 Tenczer & Stüwe (2003); 14:
1324 Gregurek *et al.* (1997); 15: Tenczer *et al.* (2006); 16: Janak *et al.* (2009); 17:
1325 Putis *et al.* (2002); 18: Neubauer *et al.* (1999); 19: Torok (1999) and Torok
1326 (2003); 20: Tropper *et al.* (2001).

1327 Fig. 2: Cross-sections for Eastern (AA'), Central (BB') and Western (CC')
1328 Alps redrawn after Polino *et al.* (1990), Dal Piaz *et al.* (2001) and Schus-
1329 ter *et al.* (2004). In the Central Alps cross section the lower austroalpine
1330 comprises slices of basement units of the Err and Bernina systems, interlay-
1331 ered with thin slivers of Mesozoic sediments (e.g. Froitzheim *et al.*, 1994),
1332 giving rise to a complex setting characterised by the repetition of cover and
1333 basement lithostratigraphic units.

1334 Fig. 3: P/T ratios and peak ages obtained from the collection of natural
1335 data (Tables 1 and 2).

1336 Fig. 4: Peak $P-T$ estimates obtained from the natural data collected for the
1337 Western (a), Central (b) and Eastern (c) Austroalpine; the numbers refer to
1338 locations marked in Fig. 1. The metamorphic facies fields shown are after
1339 Ernst & Liou (2008). GS: greenschist facies; BS: blueschist facies; EP-A:
1340 epidote-amphibolite facies; A: amphibolite facies; A-E: amphibole-eclogite
1341 facies; EP-E: zoisite-eclogite facies; Lws-E: lawsonite-eclogite facies; GR:
1342 granulite facies; HGR: kyanite-granulite facies.

1343 Fig. 5: Four evolutionary stages of the model: (a) 10 Ma, (b) 20 Ma, (c)

1344 35 Ma and (d) 60 Ma. In the insets, the streamlines (blue lines) obtained
1345 in the corner area are reported. 1) Upper continental crust, 2) lower conti-
1346 nental crust, 3) upper oceanic crust, 4) lower oceanic crust, 5) sediments, 6)
1347 exhumed upper continental crust, 7) exhumed lower continental crust, and
1348 8) continental lithospheric mantle.

1349 Fig. 6: An example of a P - T - t path for a lower continental marker at four
1350 time increments; the red circle indicates the initial position of the marker,
1351 and the black circle indicates the marker location at a particular subduction
1352 age. The metamorphic facies fields are from Ernst & Liou (2008). GS:
1353 greenschist facies; BS: blueschist facies; EP-A: epidote-amphibolite facies;
1354 A: amphibolite facies; A-E: amphibole-eclogite facies; EP-E: zoisite-eclogite
1355 facies; Lws-E: lawsonite-eclogite facies; GR: granulite facies; HGR: kyanite-
1356 granulite facies.

1357 Fig. 7: Predicted peak P and T conditions recorded by the exhumed mark-
1358 ers (see the legend for the lithologic affinities) in terms of $P_{max}T$ (a) and
1359 PT_{max} (b). (c): thermal gradients in the subduction zone for seven refer-
1360 ence depths obtained from a comparison of the dynamics evolution of the
1361 isotherm configuration to the thermal gradients obtained by the burial paths
1362 of two markers (blue = upper continental crust; green = lower continental
1363 crust). (d): The P/T ratio obtained based on P/T ratio obtained by the
1364 mean $P_{max}T$ conditions recorded by the exhumed markers for five different
1365 time steps. a): Upper continental crust and b): lower continental crust.

1366 Fig. 8: Comparison of the natural P - T peak assemblages coming from

1367 the Austroalpine of the Western Alps (blue dots) and simulated $P_{max}T$ and
1368 PT_{max} data (grey dots) for slices ablated from upper (a-c) and lower (b-d)
1369 continental crust. e) $P-T$ peak assemblages obtained for the peak age of
1370 SLZ (blue dots) and f) for the External Slices (blue dots) compared to the
1371 natural estimates (shaded area). The orange dots represent the simulated
1372 $P-T$ data at the end of the subduction period (30 Ma), which is interpreted
1373 as the exhumation age.

1374 Fig. 9: Comparison of the simulated and natural $P-T-t$ paths inferred for the
1375 Austroalpine. See caption of Fig. 1 for the reference numbers. Pre-Alpine
1376 $P-T-t$ path references are 10: Lardeaux & Spalla (1991); 25: Lardeaux
1377 & Spalla (1991) and Rebay & Spalla (2001); 34: Kienast & Nicot (1971),
1378 Gardien *et al.* (1994) and Roda & Zucali (2008); 01: Gazzola *et al.* (2000)
1379 and 19.2: Schuster *et al.* (2001).

1380 Fig. 10: Comparison of the natural $P-T$ peak assemblages coming from
1381 the Austroalpine of the Central Alps (red dots) and simulated $P_{max}T$ and
1382 PT_{max} data (grey dots) for slices ablated from upper (a-c) and lower (b-d)
1383 continental crust. e): $P-T$ peak assemblages obtained for the peak age of
1384 the Central Austroalpine (red dots) compared with the natural assemblages
1385 (shaded area). The orange dots represent the $P-T$ data for the period from
1386 50 to 35 Ma, which is interpreted as the exhumation age.

1387 Fig. 11: Comparison of the natural $P-T$ peak assemblages coming from
1388 the Austroalpine of the Eastern Alps (green dots) and simulated $P_{max}T$ and
1389 PT_{max} data (grey dots) for slices ablated from upper (a-c) and lower (b-d)

1390 continental crust. e) and f): P - T peak conditions predicted after 30–40 Ma
1391 from the beginning of subduction obtained for the two different starting ages
1392 of the simulation: 130 Ma (e) and 100 Ma (f) compared to natural estimates
1393 (shaded area). The red and orange dots represent the P - T data at two
1394 times from the start of the subduction and are interpreted as two natural
1395 exhumation ages (80 Ma red; 50 Ma orange).

FIGURES

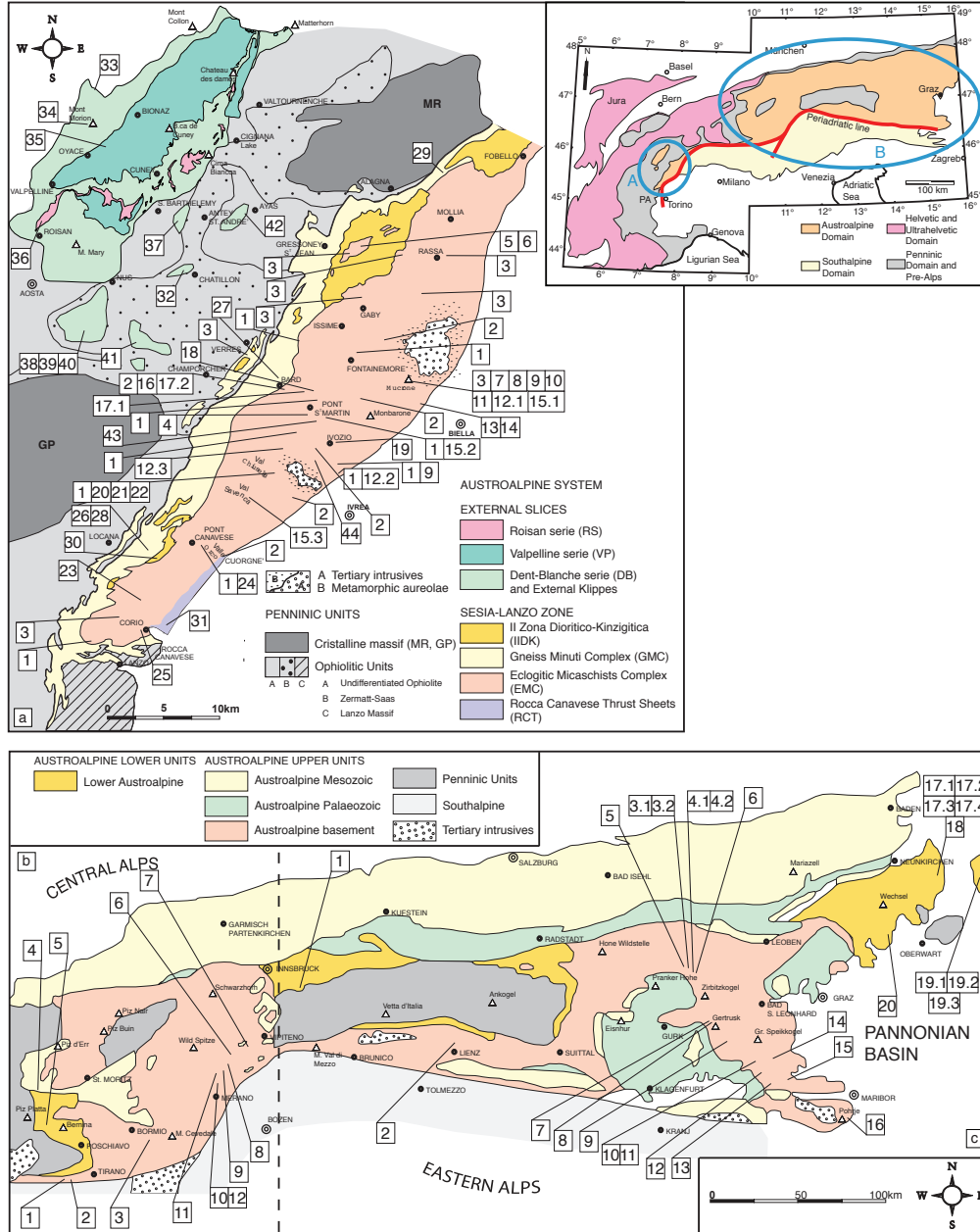


Fig. 1

1396

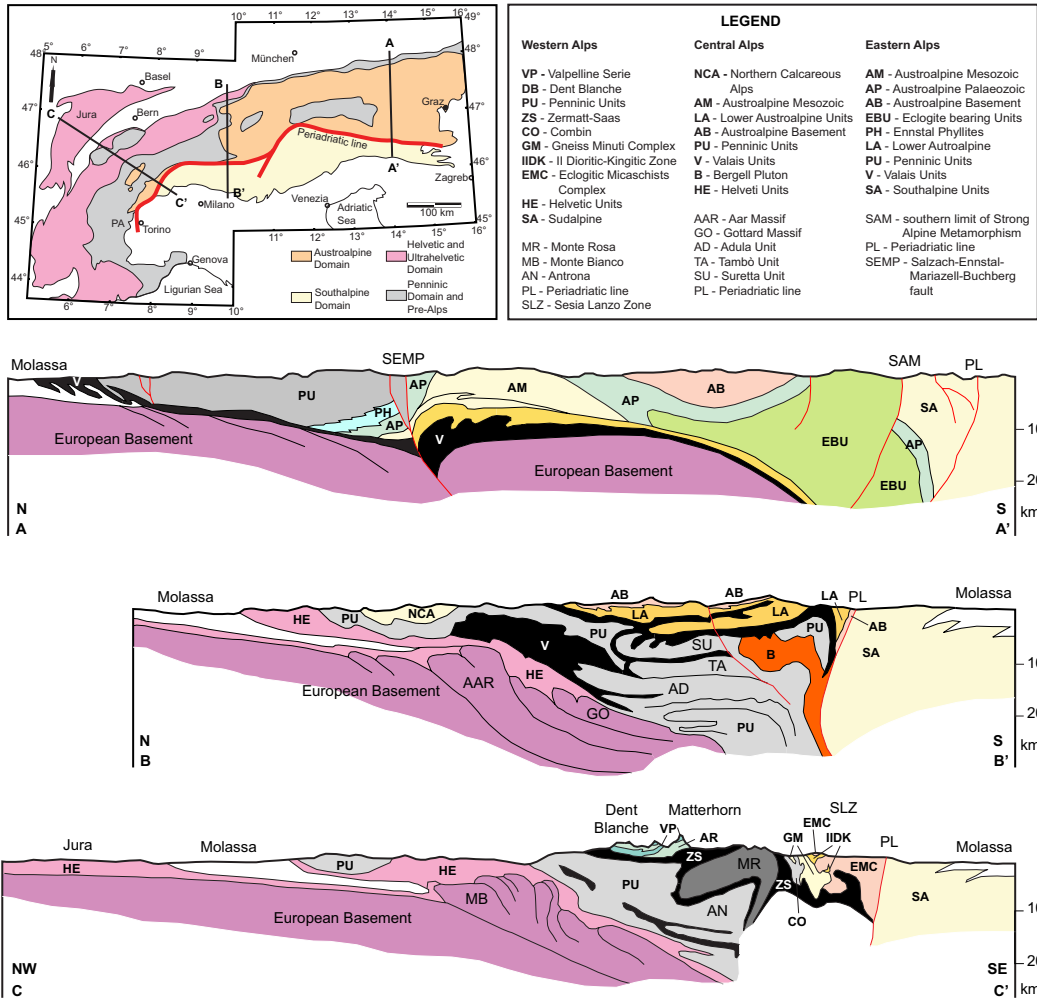


Fig. 2

1397

1398

1399

1400

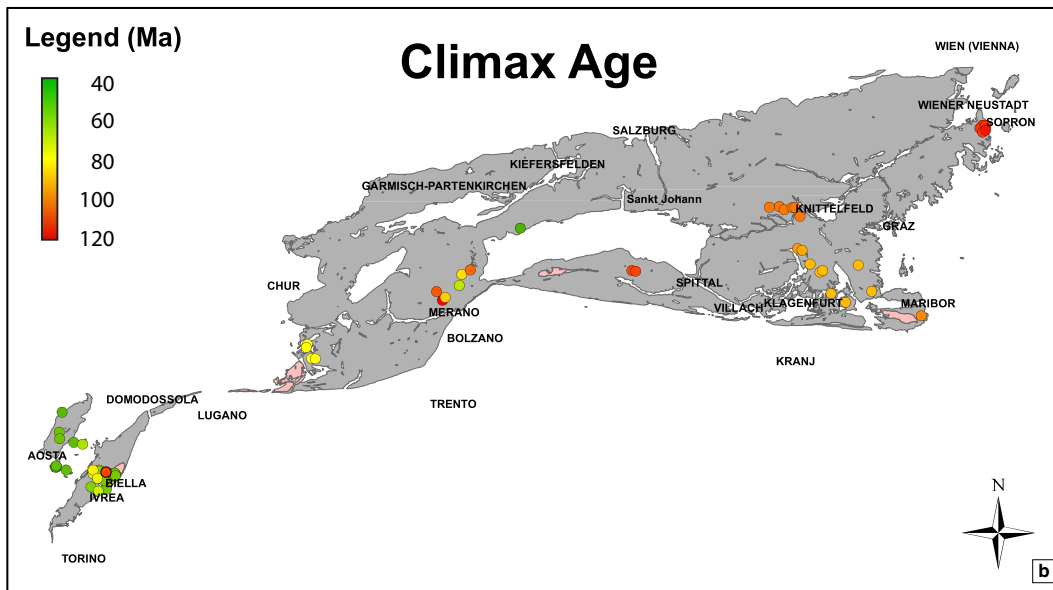
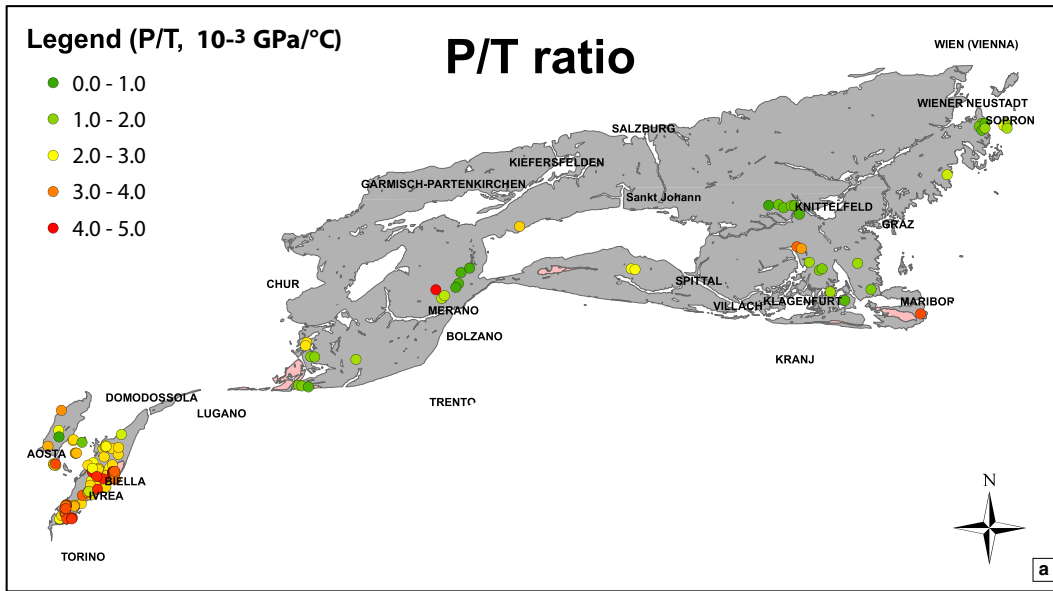


Fig. 3

1401

1402

1403

1404

1405

1406

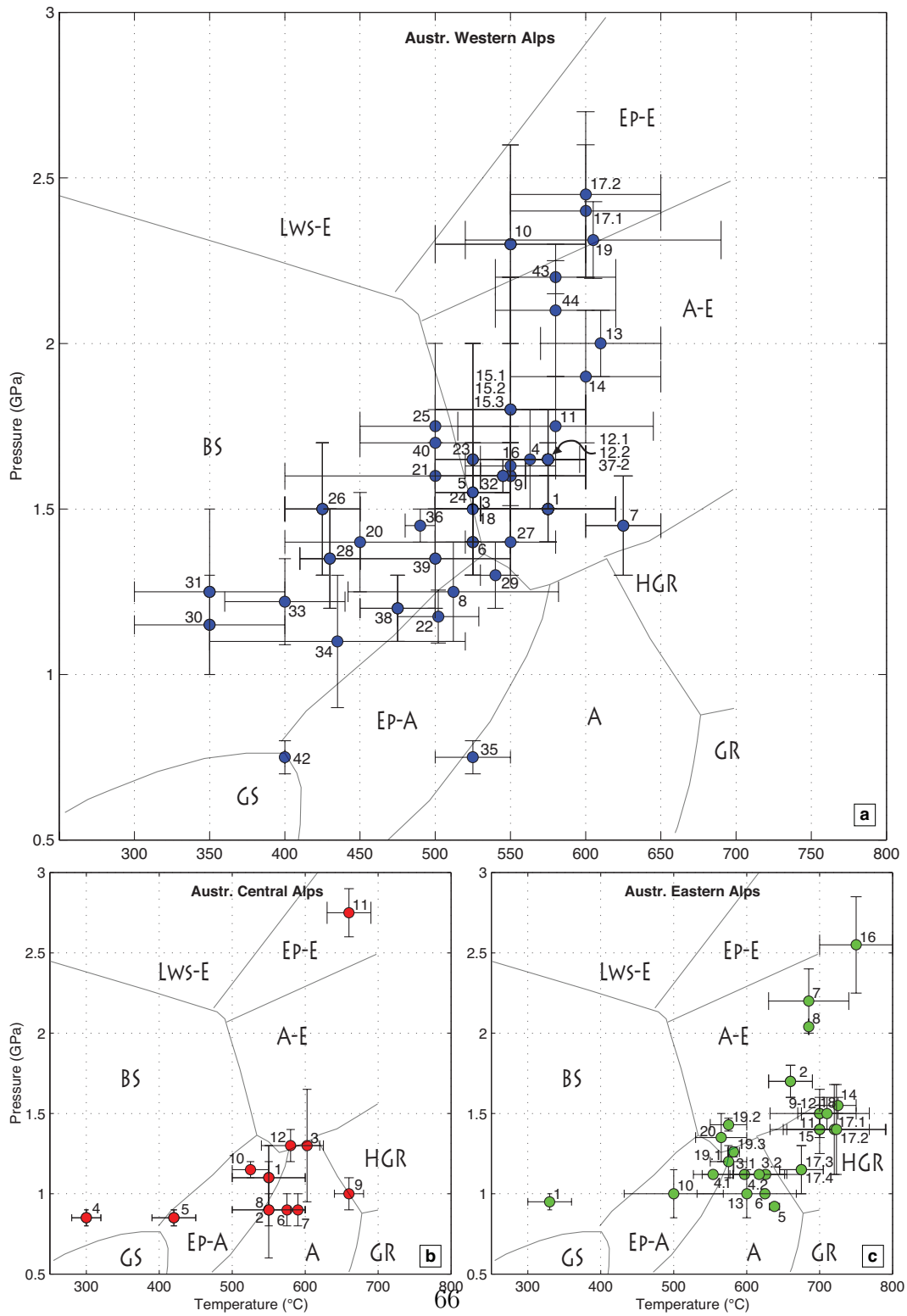


Fig. 4

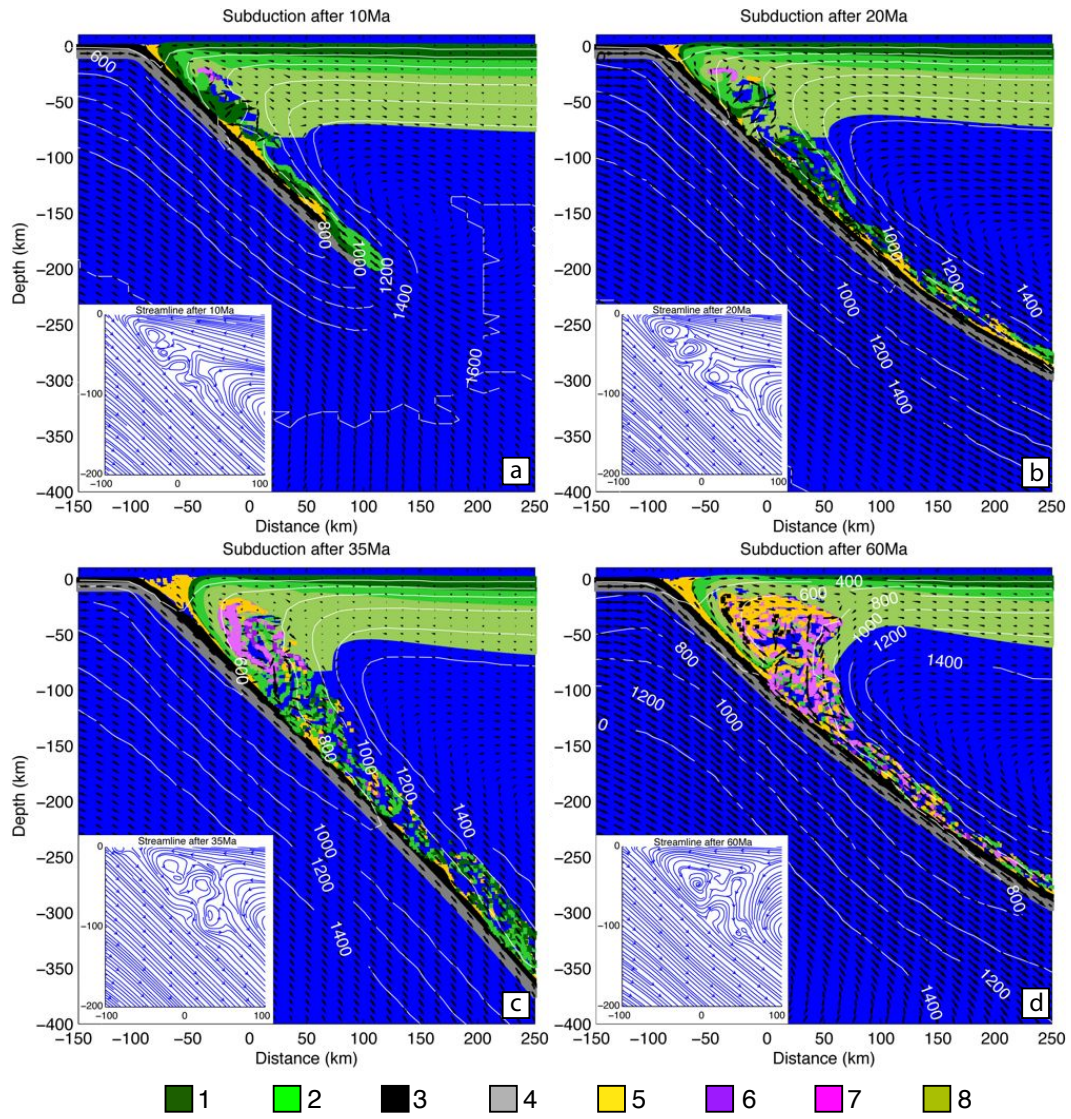


Fig. 5

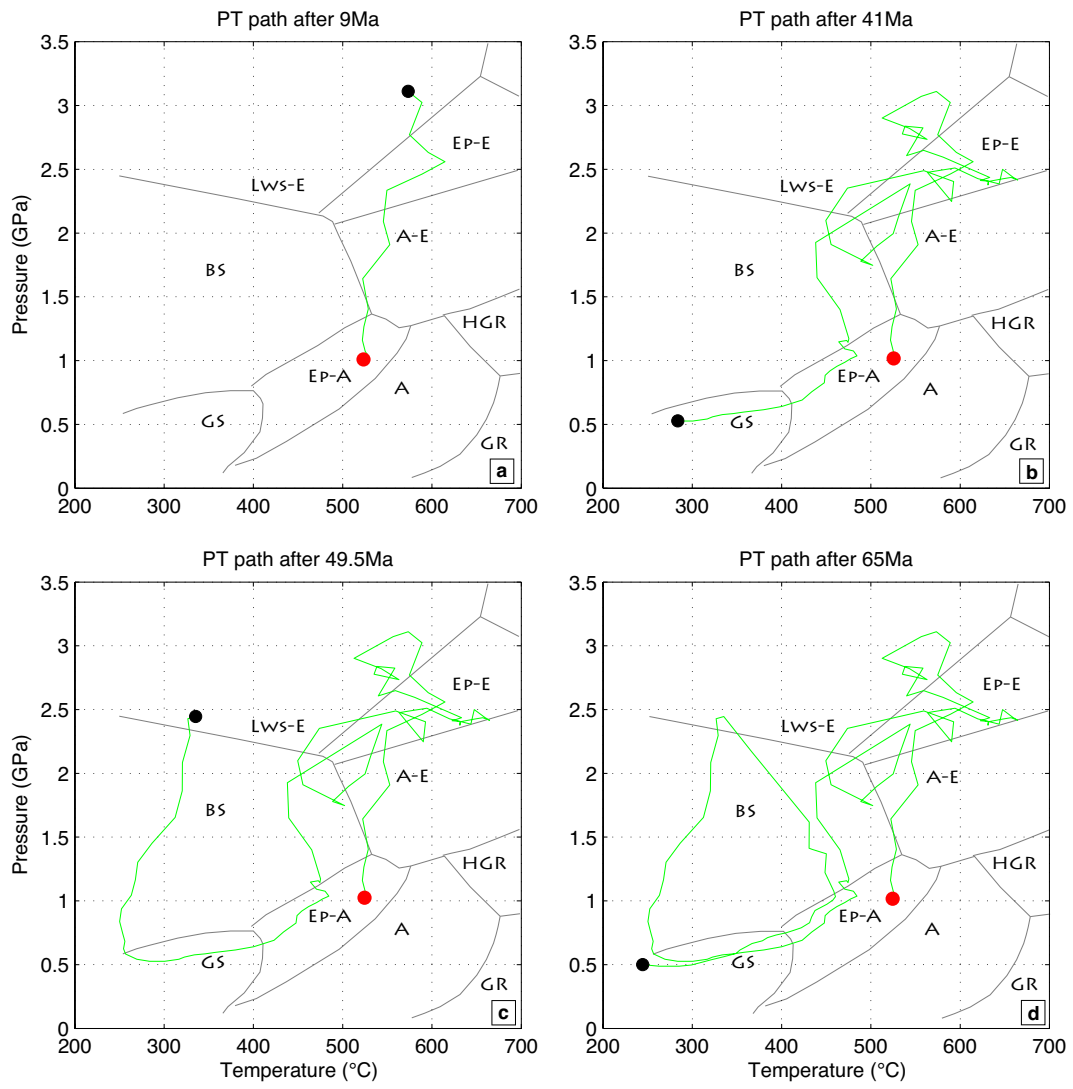


Fig. 6

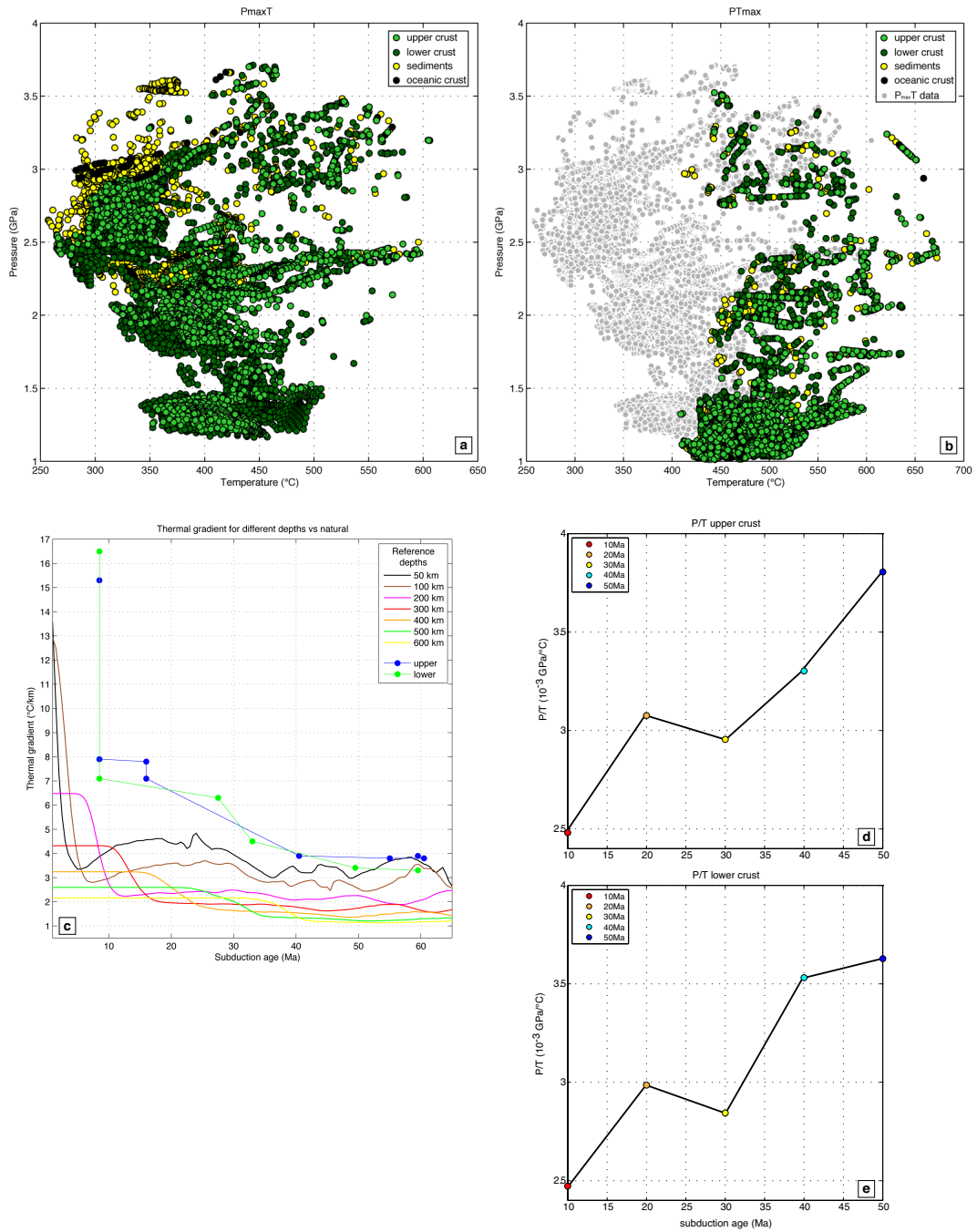


Fig. 7

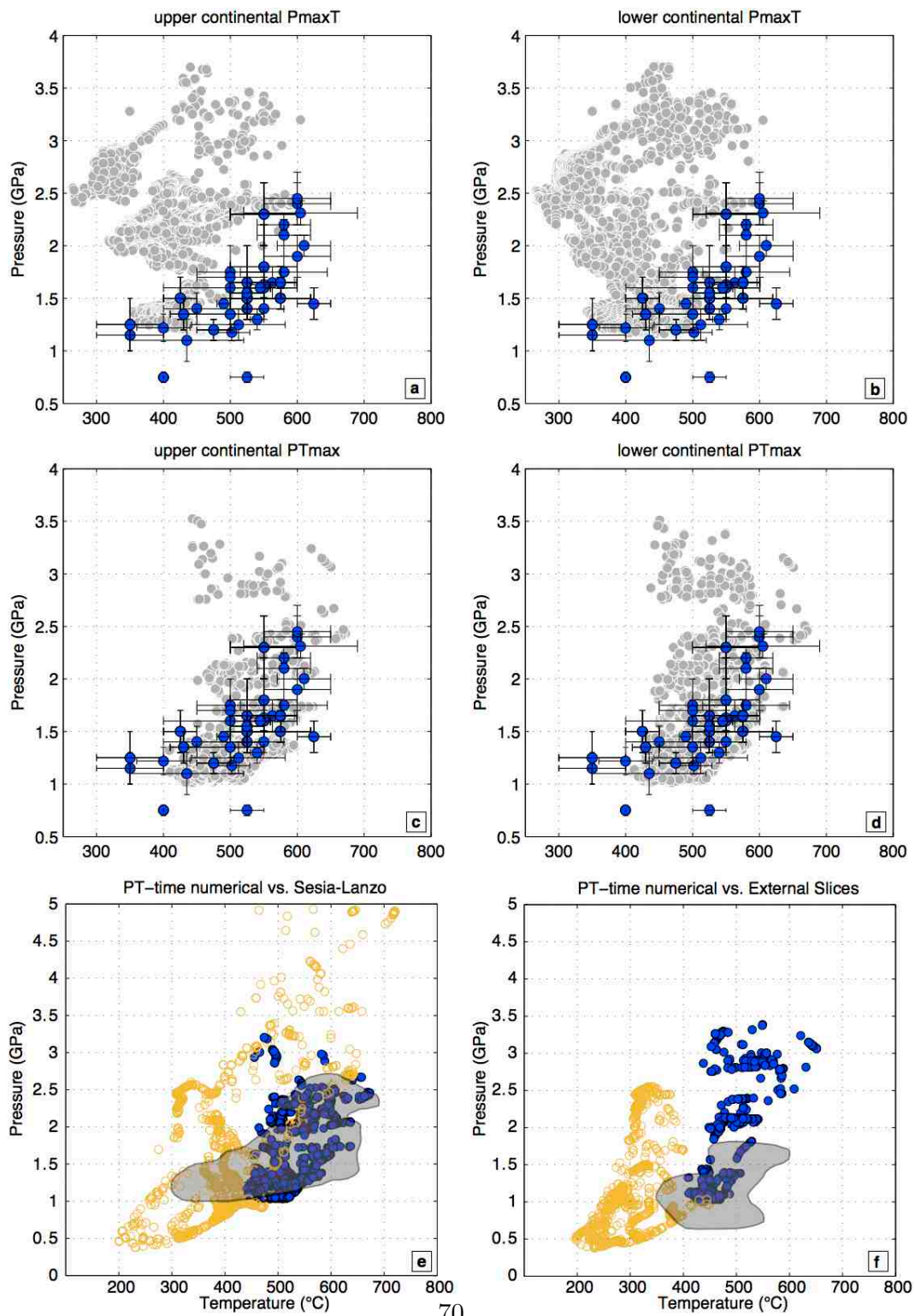


Fig. 8

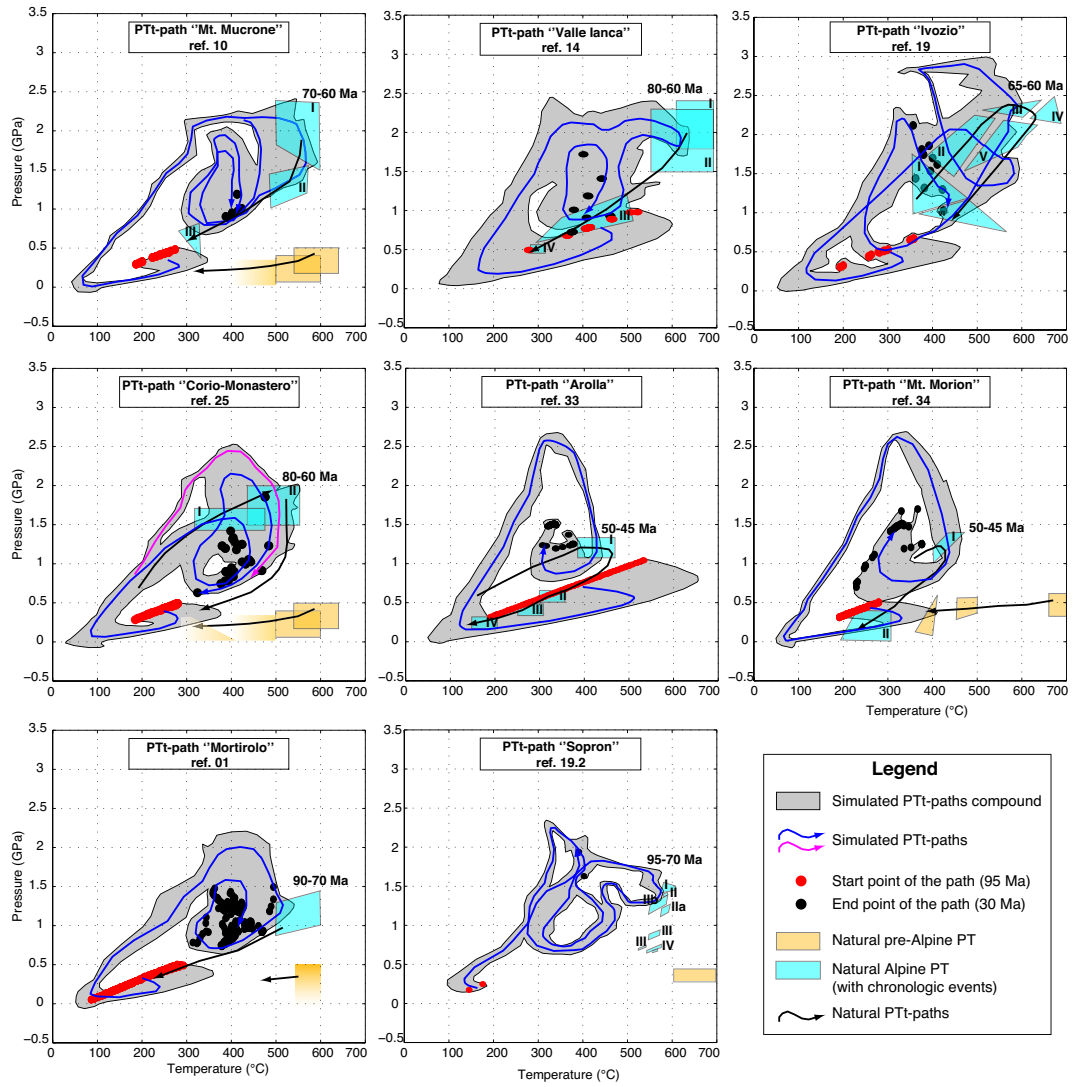


Fig. 9

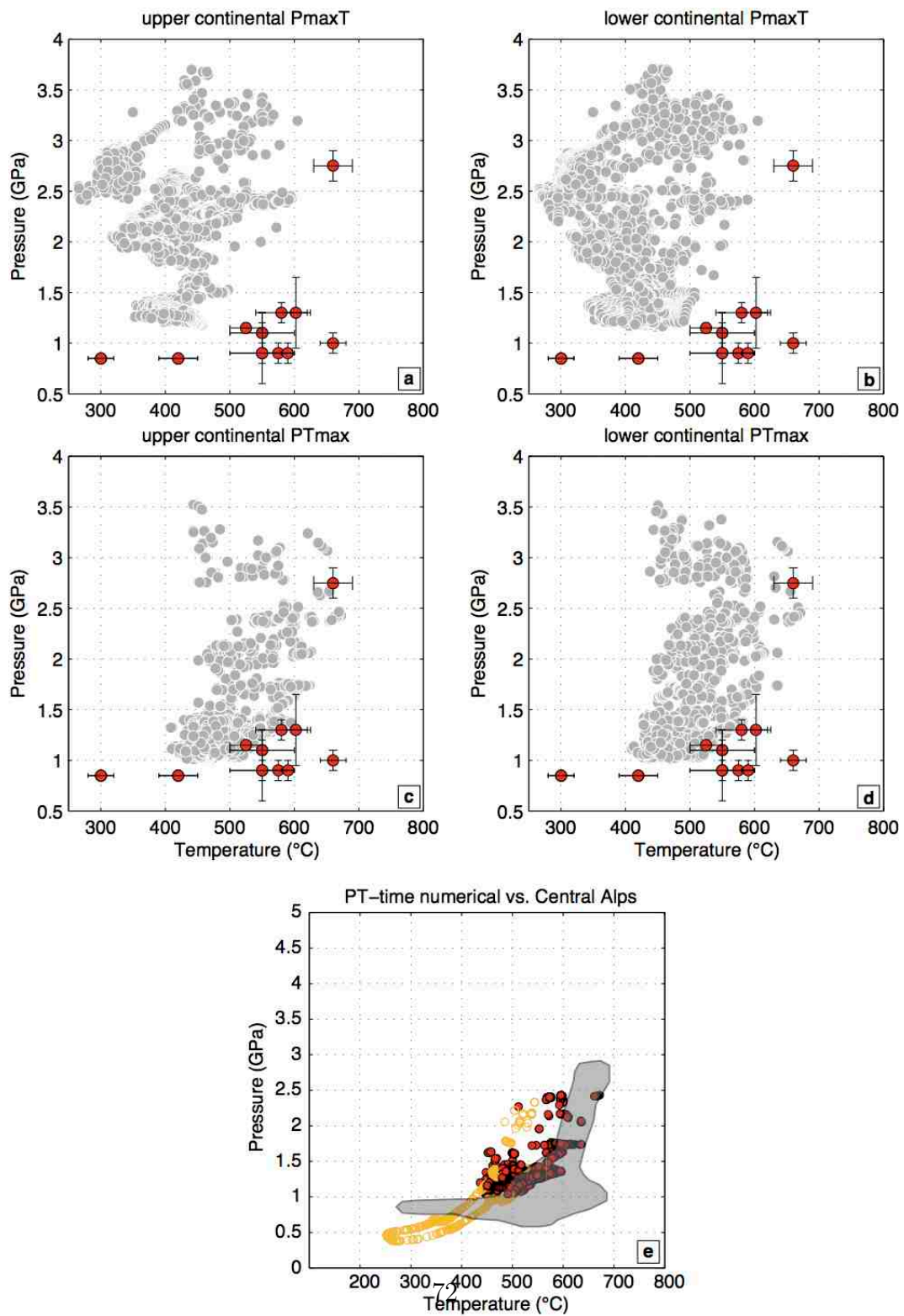


Fig. 10

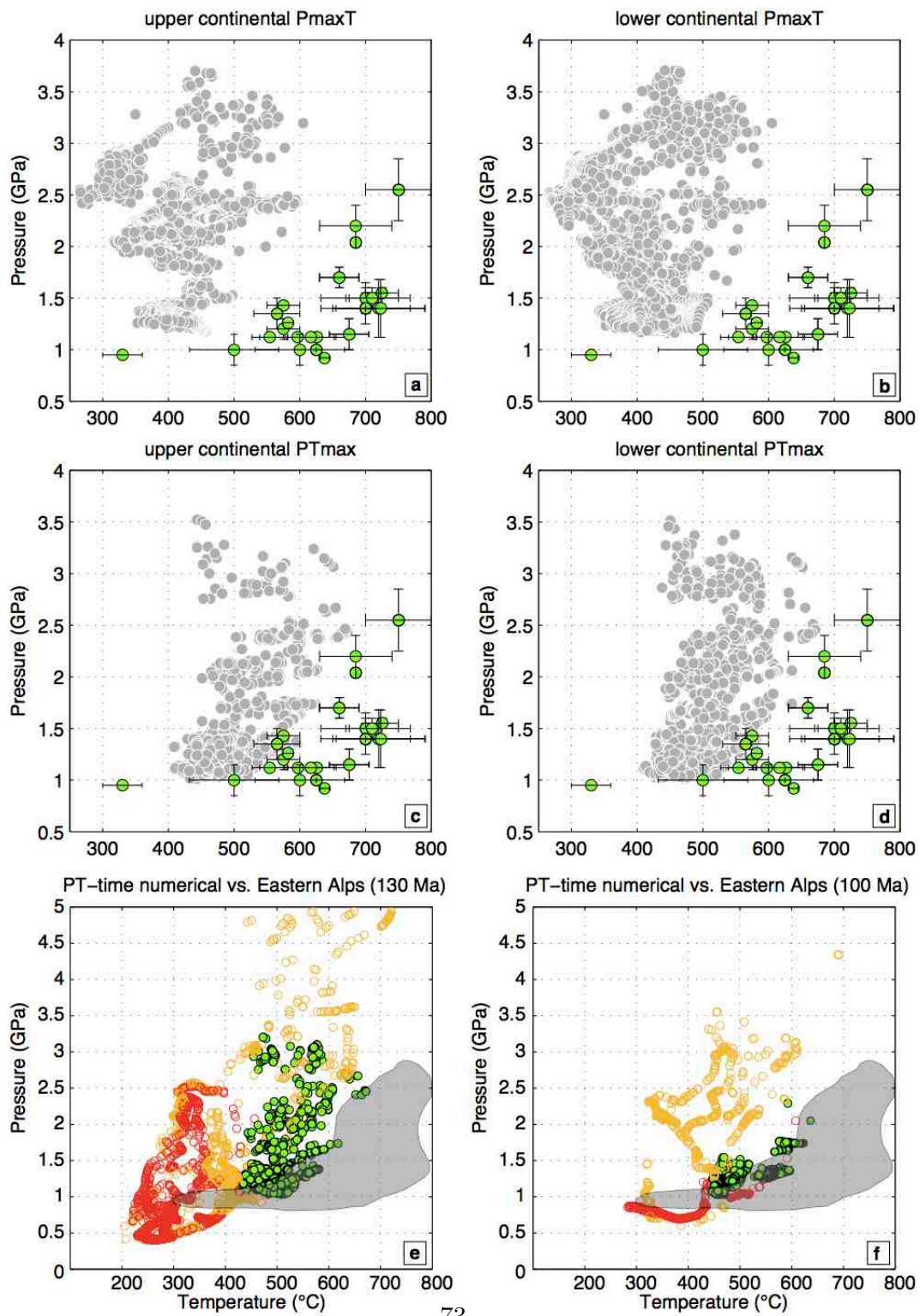


Fig. 11

Table 1: Climax ages for the Austroalpine of the Western Alps: EMC Eclogite Micaschists Complex; GM Gneiss Minuti; II DK II Zona Dioritico-Kinzigitica; RCTS Rocca Canavese Thrust Sheet; CH Chatillon; *DB* Dent-Blanche; VP Valpelline; RS Roisan; EL Etirol-Levaz; EM Emilius; GL Glacier-Rafraay; PK Pillonet Klippe. Keys correspond to the references and locations on Fig. 1a.

Key	Locality	Nappe Met. C.	Climax age (Ma)	Method	References
4	Lower VdA	EMC	65.0±5.0	zircon	Rubatto <i>et al.</i> (1999)
7	Mt. Mucrone	EMC	71.2±3.2	Rb/Sr	Hunziker (1974)
			118.0±2.3	Ar/Ar	Hy (1984)
8	Mt. Mucrone	EMC	129.0±15.0	Rb/Sr	Oberhänsli <i>et al.</i> (1985)
			114.0±1.0	Rb/Sr	Oberhänsli <i>et al.</i> (1985)
9	Lower VdA	EMC	69–90	Rb/Sr	Hunziker (1974)
	Mt. Mucrone				
12.1	Mt. Mucrone	EMC	65.0±5.0	zircon	Rubatto <i>et al.</i> (1999)
			66–88	allanite	Cenki-Tok <i>et al.</i> (2011)
12.2	Lower VdA	EMC	65.0±3.0	zircon	Rubatto <i>et al.</i> (1999)
12.3	Cima di Bonze	EMC	68.0±7.0	zircon	Rubatto <i>et al.</i> (1999)
15.2	Montestrutto	EMC	≥80	Ar/Ar	Stöckhert <i>et al.</i> (1986)
16	Bard	EMC	70–90	Rb/Sr	Hunziker (1974)
18	Marine	EMC	≥69.4±0.7	Ar/Ar	Ruffet <i>et al.</i> (1995)
19	Ivozio	EMC	65.0±3.0	zircon	Rubatto <i>et al.</i> (1999)
27	Lower VdA	GM	≥45–60	Rb/Sr	Hunziker <i>et al.</i> (1992)
			≥60–85	K/Ar	Hunziker <i>et al.</i> (1992)
33	Arolla	DB	36.0±4.0	K/Ar	Ayrton <i>et al.</i> (1982)
			41.0±0.3	Ar/Ar	Cosca <i>et al.</i> (1994)
34	Mt. Morion	DB	46.0±1.5	Rb/Sr	Ayrton <i>et al.</i> (1982)
35	Valpelline	VP	46.0±1.5	Rb/Sr	Ayrton <i>et al.</i> (1982)
37	Etirol-Levaz	EL	45.0±0.7	Rb/Sr	Dal Piaz <i>et al.</i> (2003)
			47.0±0.9	Rb/Sr	Dal Piaz <i>et al.</i> (2003)
39	Mt. Emilius	EM	40.0±0.5	Rb/Sr	Dal Piaz <i>et al.</i> (2003)
			49.0±0.5	Rb/Sr	Dal Piaz <i>et al.</i> (2003)
41	Glacier-Rafraay	GL	45.0±0.4	Rb/Sr	Dal Piaz <i>et al.</i> (2003)
42	Ayas	PK	74.0±1.0	Rb/Sr	Cortiana <i>et al.</i> (1998)
43	Quincinetto	EMC	78.5±0.9	zircon	Rubatto <i>et al.</i> (2011)
44	Brosso	EMC	76.8±0.9	zircon	Rubatto <i>et al.</i> (2011)

Table 2: Climax ages for the Austroalpine of the Central-Eastern Alps: UA Upper Austroalpine; LA Lower Austroalpine. Keys correspond to the references and locations on Fig. 1b (Central Alps) and Fig. 1c (Eastern Alps).

Key	Locality	Nappe Met. C.	Climax age (Ma)	Method	References
Central Alps					
4	Maloja	LA/Err	76–89	K/Ar	Handy <i>et al.</i> (1996)
5	Engadina	LA/Margna	60–80	Rb/Sr	Frey <i>et al.</i> (1974)
			60–80	K/Ar	Frey <i>et al.</i> (1974)
6	Moos	UA/Schneeberg	84.5±1.0	Ar/Ar	Konzett & Hoinkes (1996)
7	Schneeberg	UA/Schneeberg	91.5–96.3	Sm/Nd	Habler <i>et al.</i> (2001)
8	Monteneve	UA	≥76.1±4.8	Rb/Sr	Solva <i>et al.</i> (2001)
		Texel G.	≥83.2±2.9	Ar/Ar	Solva <i>et al.</i> (2001)
10	Saltaus	UA/Texel G.	143.0±2.0	Rb/Sr	Hoinkes <i>et al.</i> (1991)
11	Ulfas	UA	84.0±5.0	U/Pb	Zanchetta (2007)
		Texel G.	≥95.0±5.0	Sm/Nd	Solva <i>et al.</i> (2005)
12	Saltaus	UA/Texel G.	85.2±4.6	Sm/Nd	Habler <i>et al.</i> (2006)
Eastern Alps					
1	Reckner	LA/Reckner N.	49.5–51.8	Ar/Ar	Dallmeyer <i>et al.</i> (1997)
2	Schober	UA/Schobergruppe	87–115	Sm/Nd	Linner (1999)
3	Mur Valley	UA/Woelz C.	92.4±14.4	Sm/Nd	Schuster & Frank (1999)
7	Kupplerbrunn	UA/Saualpe	91.1±1.3	Sm/Nd	Thöni <i>et al.</i> (2008)
8	Saualpe	UA/Saualpe	90.0±3.0	Sm/Nd	Thöni & Miller (1996)
15	Koralpe	UA/Koralp C.	87.5±4.5	Sm/Nd	Miller & Thöni (1997)
16	Pohorje	UA/Koralp C.	92.0±0.5	U/Pb	Janak <i>et al.</i> (2009)
17	Sieggraben	UA/Sieggraben C.	≥103.0±14.0	U/Pb	Putis <i>et al.</i> (2000)
18	Sieggraben	UA/Sieggraben C.	≥136–108	Ar/Ar	Dallmeyer <i>et al.</i> (1996)

Table 3: Material properties used for the simulations. References: (a) (Ranalli & Murphy, 1987), (b) (Kirby, 1983), (c) (Chopra & Peterson, 1981), (d) (Karato & Wu, 1987), (e) (Dubois & Diament, 1997; Best & Christiansen, 2001), (f) (Haenel *et al.*, 1988), (g) (Gerya & Stockhert, 2002).

Materials	Rheology	$\mu^0 (Pa s^{-1})$	n	$\rho_0 (kg/m^3)$	k(W/mK)	$H_r (\mu W/m^3)$	E(KJ/mol)	Refs.
Continental crust	dry granite	$3.47 \cdot 10^{21}$	3.20	2640	3.01	2.50	123	a,e,f
Oceanic crust: upper	10^{19}			2961	2.10	0.40	260	b,e,f
Oceanic crust: lower	diabase	$1.61 \cdot 10^{22}$	3.40	2961	2.10	0.40	260	b,e,f
Sediments	10^{19}			2640	3.01	2.50	123	e,f
Dry mantle	dry dunite	$5.01 \cdot 10^{20}$	3.41	3300	4.15	0.002	444	c,e,f
Serpentinized mantle	10^{19}			3000	4.15	0.002	444	e,f,g
Water	10^{23}			1000	0.60			
Atmosphere	10^{23}			1.18	0.03			